Fluoropolymer-based 3D printable pyrotechnic compositions

By

Johannes Marthinus Grobler

Dissertation submitted in partial fulfilment of the requirements for the degree of

Master of Engineering

(Chemical Engineering)

In the Faculty of Engineering, Built Environment and Information Technology

University of Pretoria

Pretoria

November 2017

Fluoropolymer-based 3D printable pyrotechnic compositions

Student: Johannes Marthinus Grobler

Supervisor: Prof. Walter W. Focke

Department of Chemical Engineering

University of Pretoria

Degree: Masters of Engineering (Chemical Engineering)

Abstract

The work herein covers the complete process for development, production and testing of a melt processable pyrotechnic composition, with the goal of using the composition as a printing material in a fused deposition modelling (FDM) type 3D printer. 3D printing is fast becoming an area of interest for energetic materials research. This is due to the role that geometry can play in combustion performance of a composition and 3D printing's ability to produce a variety of complex designs.

Melt processable fluoropolymers were selected as oxidisers. The polymers selected for the study were FK-800® and Dyneon 31508®. Both are co-polymers of vinylidene fluoride (VDF) and chlorotrifluoroethylene (CTFE). Aluminium was the choice fuel in this instance as it had better energetic performance than the alternatives investigated. It was also deemed to be a safer fuel when considering the combustion products. Hazardous combustion products like hydrofluoric and hydrochloric acid could be suppressed by increasing the fuel loading to 30 wt.%, thereby reducing the risks associated with burning the composition.

Preliminary differential thermal analysis (DTA) analysis indicated that the compositions would only ignite above 400 °C which was well above the suggested processing temperature of 230 °C as determined from thermogravimetric (TGA) analysis. These thermal analysis techniques indicated that the reactions were most likely a gas-solid reactions due to ignition temperatures being significantly lower than those associated with phase changes occurring in the fuels tested, yet above the decomposition temperatures for the oxidisers.

Extrusion of the compositions proceeded with addition of LFC-1® liquid fluoroelastomer. This addition was made in order to order to lower the melt viscosity, thereby improving the quality of the filament produced. Compositions were extruded with an aluminium loading of 30 wt.%. Oxidiser and LFC-1® made up the rest of the mass with the LFC-1® contributions being either 7 wt.% or 14 wt.%.

Burn rates, temperatures and ignition delays were all influenced by the addition of LFC-1® to the system. FK-800® was found to be a better oxidiser in this instance since its burn rates were consistent especially when compared to erratic nature of the Dyneon 31508® burns. Linear burn rates for the FK-800® increased from 15.9 $mm \cdot s^{-1}$ to 18.9 $mm \cdot s^{-1}$ with the increase in LFC-1® loading. Combustion temperature also increased by approximately 180 °C from 794 °C.

Printing with the material was achieved only after significant alterations were made to the hot end used. Printing proceeded in a staged, start-stop manner. After each new layer of material was deposited the printer was cleared of material and the hot end was allowed to cool. If this procedure was not followed it led to significant preheating of the material within the feeding section of the extruder. This premature heating caused feeding problems due to softening and swelling of the material within the cold side of the hot end which led to blockages, leading to the conclusion that the composition was not compatible with the off-the-shelf hot end used in this study. Low quality printing could be achieved with both FK-800® and Dyneon 31508® compositions. This would suggest that slight compositional changes paired with the alterations made to the hot end could improve the quality of the prints to an extent that would be comparable to that of more commonplace printing materials.

Keywords: Additive manufacturing; Pyrotechnics; Melt processable pyrotechnics; Laser ignition

Acknowledgments

Firstly family, Judy and Jannes, thank you for your genetic contribution. I think I turned out ok. Their significant others, Chris and Wendy, thanks for putting up with me all of these years. To all of you, thank you for the support over the course of my studies. The brother, Ihan, thank you for all the distractions.

To my supervisor, Prof. Walter Focke: Thank you for the opportunity and subsequent support and guidance. Working with you has been a great experience.

Dr. Tichapondwa, I definitely kept you from your own work at times when looking for answers. Thank you for the patience and guidance over the course of the project.

Suzette, without your specialised skill set this project and many others would be drastically extended. I really appreciate all the support.

To my colleagues at the Institute of Applied Materials, Stefan, Desania, Craig and Andrew, we had some good times, bad ideas and at times terrible results.

Thank you to AEL Mining Services, and in particular George Labuschagne and Craig Rimmington, for financial and technical support for this project.

Table of Contents

List of tables

List of Figures

1. Introduction

Composite materials consisting of a polymer containing a reactive composition are of importance for several pyrotechnic products, such as infrared decoys and propellants (Huong et al., 2014). Usually the polymer is used as a binder. This implies that its main purpose is to provide mechanical integrity and rarely contributes favourably to the reaction. Fluoropolymers on the other hand can be used to provide a very strong oxidiser, fluorine (Huong et al., 2014). For this reason they have been implemented as reactive binders in various pyrotechnic systems.

Fluoropolymers can potentially replace traditional metal oxide based oxidisers in currently implemented pyrotechnic systems. The use of fluoropolymer oxidisers is of interest due to fluorine being the most energetic oxidiser (Agrawal, 2010). The use of appropriate fluoropolymers also provides the potential for numerous continuous polymer processing techniques to be employed.

Fluoropolymers can generally be grouped as either perfluoropolymers or partially fluorinated polymers (Teng, 2012). The difference between the two is that partially fluorinated polymers also contain other elements such as hydrogen bonded to the carbon chain. Upon decomposition both kinds will release fluorine containing compounds. If decomposition occurs at a favourable temperature fluorination of the reducing agent will take place releasing more heat leading to a self-sustained reaction.

Fluoropolymer based pyrotechnic systems are used for a variety of applications, which include destructive and propulsion based systems. In these systems the fluoropolymer acts as the oxidant. Polytetrafluoroethylene (PTFE) is widely used in these systems. This is due to its high fluorine content which is required for the high temperature oxidation-reduction (redox) reaction. Its use is paired in many instances with a binder such as poly(vinylidene fluoride-co-hexafluoropropene) (VDF-HFP). Commercially known versions are supplied under the trade names Viton (DuPont) or FC-2175 (3M) (Koch, 2012).

The fuel (reducing agents) employed for these systems are usually metals such as aluminium (Al) or magnesium (Mg). One of the earliest systems based on such a combination was the magnesium, Teflon and Viton (MTV) system (Osborne and Pantoya, 2007). Alternative fuels and fluoropolymer systems have been studied and developed with silicon (Si) as one such fuel (Yarrington and Son, 2010).

The most common technique used to manufacture MTVs is the shock gel process (Koch, 2012). In this process Viton is dissolved in a ketone-type solvent such as acetone (Koch, 2012). The magnesium and Teflon are mixed with this solution. A non-solvent such as hexane is added to the mixture in order to initiate precipitation of the dissolved polymer (Koch, 2012). The composition precipitates out as grains of fuel and oxidiser closely held together by the binder.

Extrusion can also be used to produce fluoropolymer-based systems. Extrusion of MTVs requires less solvent during processing and provides for improved mixing (Koch, 2012). In this process a suitable solvent for Viton is still used and the magnesium and Teflon are fed as solids to the extruder. The composition is usually extruded using a twin screw extruder (Koch, 2012). Extrusion allows for continuous processing of the composition as well as shaping during production by selecting an appropriately shaped die. This extrusion process does not melt the polymers mentioned. Melt processing of PTFE is not possible since heating it above temperatures of 350 °C to 400 °C initiates pyrolysis (Koch, 2012) (Hough, 1995). This makes the addition of an appropriate soluble binder such as Viton necessary in order to produce the composition.

Replacing the PTFE with another fluorinated polymer which is melt processable may obviate the need for a binder since the polymer will fill both roles of binder and oxidiser. This has several advantages over the current system as it will allow for a reduction in the use of potentially hazardous solvents as well as open up other manufacturing possibilities such as 3D printing compositions using fused deposition modelling (FDM). This technique produces an article by depositing layers of material on top of each other. Energetic materials performance is strongly influenced by the system geometry. FDM is of interest due to its ability to produce complex geometries. This means that a composition’s energetic properties may be altered by changing the structure of the print, thereby tailoring it to fit a specific purpose (Fleck et al.,

2017). FDM has been shown to be capable of assembling energetic compositions by Fleck *et al.* (2017). The system developed by them used aluminium as the fuel with poly(vinylidene fluoride) (PVDF) acting as both binder and oxidiser. It was shown that the processing of the composition did not alter its performance as long as the processing temperature was kept well below that at which degradation could occur. This development offers a wide range of opportunities for various pyrotechnic systems. This is because the internal structure of the composition can be adjusted whilst maintaining a consistent overall geometry thereby producing alternative burn pofiles for the same composition.

1.1 Problem statement

PTFE is widely used as an oxidiser due to its high fluorine content. It is however not melt processable. This means that most systems utilizing PTFE requires some other polymers to act as the binder. This limits the processability and performance of the composition depending on the binder selected. Processibility is limited by the high solids loading required. Traditionally MTV and similar systems are produced using solvents in order to assist in compounding and extrusion. Solvent-based methods have environmental and safety concerns attached to their use. This is due to the volatile emissions associated with their use.

1.2 Objective

The aim of this investigation was to produce compositions that are stable enough to be melt processed for use as a 3D printing material. This implies that they should be extrudable without requiring the assistance of solvents. This would reduce the environmental impact of production, as the use of volatile potentially hazardous compounds will be avoided. The proposed system will consist of a fluoropolymer based oxidiser, doubling as a binder, and a metal or non-metal fuel. The fluoropolymers selected for the investigation are FK-800® and Dyneon 31508®. Fuels will be fine powders in the micron range to allow for ease of compounding.

2. Literature review

2.1 Factors affecting combustion

2.1.1 Reaction

In order to process a pyrotechnic mixture the mechanism of the ignition and combustion should be understood. There are multiple stages that make up a chemical explosive event (Akhavan, 2004):

- ignition;
- deflagration;
- transition; and
- detonation.

The event can stop before detonation depending on the composition and conditions. Ignition is instigated by external factors. Heat, friction and electrical stimuli are three of the methods that can be used to initiate the reaction. If the stimulus is sufficiently intense, it will initiate pre-ignition reactions (Akhavan, 2004). Pre-ignition reactions may lead to phase changes and changes in crystallinity which are followed by self-sustained ignition (Akhavan, 2004). The minimum temperature at which these changes occur is the ignition temperature (Conkling, 1985). At this temperature the activation energy requirement has been met. The exothermic reaction will then commence in a self-sustained fashion. It will propagate through the composition if the energy it releases can overcome the activation energy of each subsequent layer. Excessive heat loss to the environment can hamper this propagation.

As stated, pyrotechnic reactions are exothermic redox reactions. This, however, does not mean that any exothermic chemical reaction will be viable. The viability of a mixture is dependent on the following two factors (Conkling, 1985):

- spontaneity; and
- reaction rate.

The spontaneity of a reaction is dependent on the change in Gibbs energy (ΔG). Which can be calculated from equation 1.

$$\Delta G = \Delta H - T\Delta S \quad (1)$$

Spontaneity requires a large but negative value of ΔG (Conkling, 1985). In order to achieve this the heat of the reaction (ΔH) should be negative. The entropy change is illustrated by (ΔS). A positive value of ΔS will indicate an increase in the disorder of the system (Conkling, 1985). System disorder generally increases as the phase changes from solid to liquid and then gas. The final element in equation 1 is the temperature (T) at which the reaction is commencing. Higher temperatures lead to the faster chemical reactions (Conkling, 1985). Other factors affecting the rate are mentioned in subsequent sections.

The heat of reaction is calculated as the difference between the heat of formation of the products and reactants. This is illustrated in equation 2.

$$\Delta H = \Delta H_{\text{f, products}} - \Delta H_{\text{f, reactants}} \quad (2)$$

An Ellingham diagram is a graphical representation of equation. An example of this diagram was generated for oxidation reactions as depicted in Figure 1. In the diagram, the normalised free energy is plotted against temperature. It consists of straight lines since heat of reaction and entropy changes are relatively constant with temperature. The slopes do change when phase changes are involved. For the components plotted Figure 1 aluminium, magnesium and calcium (Ca) have the most negative values for ΔG. Lower values of ΔG are required for fuels while higher values are favourable when selecting oxidising agents.

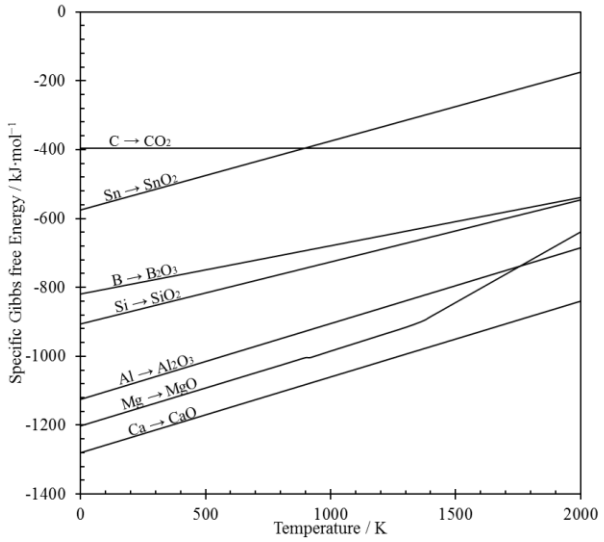

Figure 1. Ellingham diagram.

2.1.2 Pyrotechnic reaction

The pyrotechnic reaction as a whole is influenced by a variety of factors including chemical and physiochemical. These factors can further be divided into the following categories (Berger, 2005):

- type of chemicals;
- oxygen balance;
- particle size;
- binder, type and content if applicable; and
- degree of mixing.

2.1.2.1 Chemicals

The chemicals refer to the oxidisers, reducing agents, binders and retardants. Retardants are inert material added to the composition in order to adjust the combustion characteristics of the active components. This is achieved by altering the phases present, the heat of reaction, heat transfer rate and stoichiometry.

Phase changes and decomposition temperatures differ for reactants and are important factors to consider when designing a pyrotechnic system. Should high heat transfer be required (e.g. as in metal cutting), a reaction should be chosen that has condensed products. Whereas, if work is required, systems producing more gaseous products are favoured. Reaction rate is also influenced by the temperatures at which phase changes occur for the reactants and products. If one or more components undergo a phase change it increases the reactivity of the mixture (Conkling, 1985). This is due to the improved contact provided by either liquid or gas phases. For this reason melting points and or decomposition temperatures should be considered when designing a pyrotechnic mixture. If the melting temperature of the fuel is high, e.g. as that of boron (B), it will slow down the reaction rate due to a lower reactivity and this may lead to ignition difficulties (Conkling, 1985).

In other cases it has been shown that the ignition temperature is similar to the melting temperature of the oxidant (Moghaddam and Rees, 2003). The nature of the oxidant decomposition also affects the ignition temperature. Exothermic decomposition drives the

ignition temperature down while endothermic decomposition increases the ignition temperature (Agrawal, 2010).

Thermal conductivity is another aspect that is affected by the choice of fuel and oxidiser and inert materials added. It is especially important for gasless formulations. In these formulations heat can only be transferred between layers in contact with each other. This transfer is dependent on conduction (Agrawal, 2010). Materials with greater thermal conductivities will increase this transfer of energy to subsequent layers, thereby increasing the burn rate.

Good fuels will react with oxidants like oxygen or fluorine to form a stable compound and in the process release a considerable amount of heat (Conkling, 1985). Other properties of good fuels are relatively low cost, stability during storage, light weight and a high specific heat of combustion (Conkling, 1985). This excludes most of the alkali and alkaline earth metals due to their reactiveness with moisture and atmospheric oxygen. Cost somewhat limits the use of metals like titanium (Ti) and tungsten (W) (Yen and Wang, 2012). Furthermore, the toxicity of certain compounds, e.g. beryllium (Be), may preclude their use in certain applications (Yen and Wang, 2012). Magnesium and aluminium are examples of some of the most extensively used metal fuels (Conkling, 1985).

Aluminium is widely used due to its relatively low cost, its light weight and storage stability (Conkling, 1985). Aluminium powder is used in a variety of forms for pyrotechnic systems. It ranges from flakes to spheres. Spheres have the minimum surface area and thereby the lowest reactivity (Conkling, 1985). The flakes are more reactive but results will be less reproducible (Conkling, 1985). The surfaces of aluminium particles are covered by a dense adherent aluminium oxide (Al_2O_3) layer. Since aluminium is oxidised under ambient conditions, the natural oxide layer provides protection for underlying aluminium preventing further oxidation (Conkling, 1985).

Magnesium is a reactive metal which makes it a good fuel under the right conditions (Conkling, 1985). Magnesium lacks the protective oxide layer that aluminium has. It reacts with atmospheric moisture as well as certain oxidisers under ambient conditions (Conkling, 1985).

This will reduce its effectiveness as the active fuel content is continuously decreased due to oxidation of the surface layers. Coating the magnesium particles with a protective substance can extend the storage life of the mixture. An example of such a coating is potassium dichromate. The toxicity of this coating makes its use in certain environments questionable (Conkling, 1985). These problems should be taken into account when selecting oxidisers and binders for the applications illustrated in Figure 2.

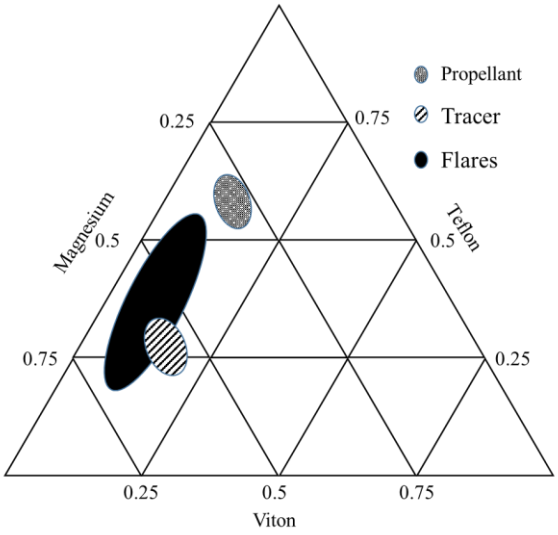

Figure 2. Compositions for different MTV applications (Koch, 2002).

Silicon and boron are examples of non-metallic fuels. Boron in fact has a higher heat of combustion than the metals mentioned but its use is limited due to ignition problems and the relatively high cost associated with it (Conkling, 1985). Silicon is widely used due to its relatively low cost and high stability (Conkling, 1985). It does however have a high melting point which can lead to ignition difficulties depending on which oxidisers it is used with.

Oxidisers are usually ionic solids (Conkling, 1985). These decompose during the reaction releasing oxygen. This released oxygen is then free to react with the fuel. Some examples are metal oxides, nitrates and sulfates. Halogenated compounds, like certain polymers, have also found use as oxidisers. The halogens (fluorine or chlorine) released during decomposition of these compounds react exothermally with the fuel. Fluoropolymers like PTFE are of great interest. This is due to the fact that fluorine is an excellent oxidising agent. Fluorine readily acquires donated electrons since it is the most electronegative element. Fluoropolymers can

partially or completely replace oxygen containing oxidisers in pyrotechnic compositions. Table 1 compares oxidation with fluorination for several fuels.

Table 1. Comparison of oxidisers with various fuels

Fuel	Melting point (°C)[a]	Boiling point (°C)[a]	Oxidation		Fluorination	
			ΔH_f (kJ·g^{-1})[b]	Combustion product	ΔH_f (kJ·g^{-1})[c]	Fluorination product
Al	660	2467	-16.38	Al_2O_3	-17.98	AlF_3
Mg	649	2750	-14.93	MgO	-18	MgF_2
Ti	1660	3287	-11.79	TiO_2	-13.69 -13.31	TiF_3 TiF_4
W	3410	5660	-3.53	WO_3	-5.75	WF_6
Zr	1852	4377	-8.79	ZrO_2	-9.73 -11.43	ZrF_3 ZrF_4
B	2300	2550	-18.15	B_2O_3	-16.77	BF_3
Si	1410	2355	-14.13	SiO_2	-15.51	SiF_4

[a](Conkling, 1985), [b](Poling et al., 2008), [c](Koch, 2012)

It is clear that in most cases the heat of formation for metal fluorides is higher than that of the metal oxides. Illustrating the benefit of using fluorine containing compounds as an oxidiser should the source of the fluorine have a favourable ΔH_f.

2.1.2.3 Oxygen balance

Pyrotechnic mixtures can range from fuel lean to fuel rich. The ratio in which the fuel and oxidiser are mixed will affect the reaction rate as well as the heat of the reaction. Both of these will be maximised at different fuel loadings.

The heat of reaction is at a maximum when the mixture has a stoichiometric ratio (Berger, 2005). It is possible that this will not coincide with the ratio for maximum reaction rate. Higher fuel loading tend to increase the burning rate but it will also reduce the adiabatic flame temperature (Kubota and Serizawa, 1987). For certain applications the increased burn rate will be more beneficial than optimal energy output.

2.1.2.4 Particle size and active surface area

As mentioned reductions in the particle size of constituents increase the reaction rate of a pyrotechnic composition. This is due to the increase in surface area to volume ratio. As particle size decreases the ratio of atoms on the surface of the particle to that of the bulk increases. This is illustrated in Figure 3 for spherical iron crystals.

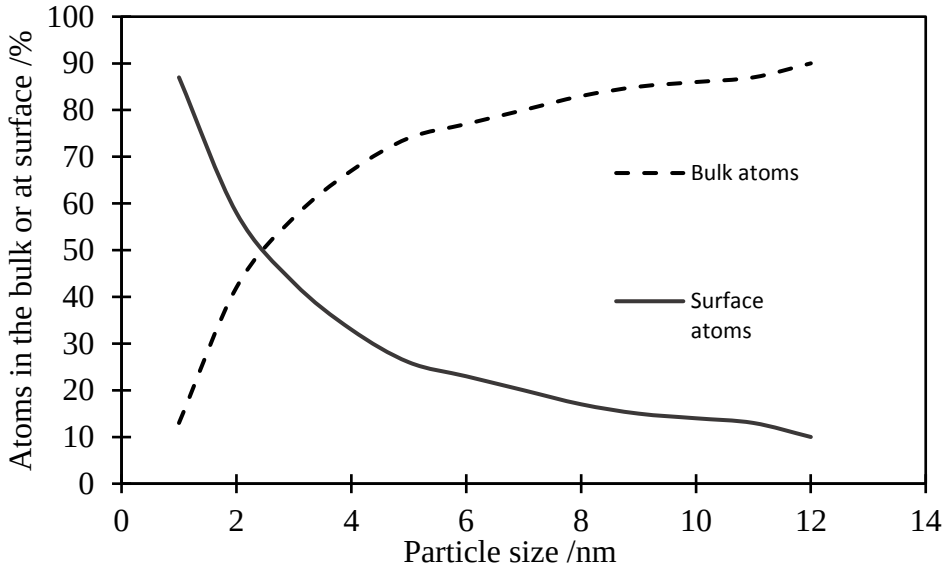

Figure 3. Distribution of atoms for spherical iron crystals (Yetter et al., 2009).

An increase in specific surface area leads to an increase in reactivity. However, it does not influence the heat of the reaction (Berger, 2005). This increase in reactivity may be due to a lowering of melting and ignition temperatures (Terry et al., 2014) caused by the increased fraction of surface atoms relative to the bulk. Reactivity changes because there is a difference between the electrical and thermo-chemical properties of the bulk and surface atoms (Yetter et al., 2009). As the surface to bulk ratio increases the bulk atoms will start to exhibit properties of the surface atoms (Yetter et al., 2009).

This effect is becomes more prominent as particles approach the nanoscale. Melting temperatures of nanoscale particles are much lower than that of their micron-sized counterparts with differences being as large as 300 K (Pantoya and Granier, 2005). Increased reaction rates are attributed to increased surface contact between the fuel and oxidiser particles. This is due to the reaction being mostly diffusion controlled, which will be aided by increased surface contact (Pantoya and Granier, 2005). The reduction in particle size can also lead to a worsening of performance due to a reduction in the active fuel content. An oxide layer covers the surface of fuels like aluminium and passivation corresponds to a certain thickness that is independent of particle size. As particles get smaller the significance of this layer and its effects on the system will increase. This is especially true for nano-fuels where the reduction in the active fuel content can be significant (Pantoya and Granier, 2005). Alternatively the oxidiser particle size can be reduced to provide similar benefits without reducing the active fuel content (Weismiller et al., 2011). A comparison of micron- and nanosized fuels and oxidisers are shown in Table 2.

Table 2. Effects of changing relative size of the fuel and the oxidiser for aluminium based thermites (adapted from Weismiller *et al*. (2011)).

Components	**Component sizes**		**Linear burn rate**	**Mass burn rate**	**Mass % Al_2O_3**
	Al	**Oxide**	**($m \cdot s^{-1}$)**	**($kg \cdot s^{-1}$)**	
Al/CuO	Nano	Nano	980	3.8	17
	Micron	Nano	660	4.8	1
	Nano	Micron	200	1.3	17
	Micron	Micron	180	2	1
Al/MoO_3	Nano	Nano	680	2	26
	Micron	Nano	360	1.5	1.7
	Nano	Micron	150	0.45	26
	Micron	Micron	47	0.52	1.7

For both compositions compared in Table 2 the highest burn rates were achieved when both the fuel and the oxidiser where in the nanometer range. When only one component was in the nanometer range the systems which utilised oxidisers in that range outperform those with nano-fuels. As mentioned earlier the active fuel content is affected by the particle size reduction. This is evident in the clear increase in the mass fraction of aluminium oxide in the systems containing nano-aluminium as fuel. It has been determined that aluminium oxide acts as an inert diluent, that reduces both the reaction rate and temperature as it alters the fuel oxidiser ratios (Weismiller et al., 2011). For this reason it needs to be accounted for when designing a system.

Alternatively the active surface area of a substance can be increased by porosification. This process has been shown to increase burn rate of micron-sized fuels. Micron-sized porous fuels have the added benefit of a proportionally lower oxide content. It can even be oxide free depending on the production procedure used. The lack of an oxide layer can drastically improve the reactivity of the fuel.

2.1.2.5 Binders

Pyrotechnic compositions consisting of fine powders are held together by binders for certain applications (Berger, 2005). Binders consist of either natural products or synthetic polymers (Agrawal, 2010). The binder type as well as its loading can have a significant influence on the heat of reaction as well as the reaction rate (Berger, 2005). This is due to the binder changing the fuel oxidiser ratio (Conkling, 1985). The heat of combustion of the binder also affects the combustion performance of the mixture (BariSin and BatiniC-Haberle, 1994). The influence the binder type has on a 35 wt.% aluminium, 40 wt.% potassium perchlorate ($KClO_4$), 20 wt.% barium nitrate ($Ba(NO_3)_2$) and 5 wt.% binder pyrotechnic composition are illustrated in Table 3.

Table 3 shows that the type of binder has an impact on the ignition temperature of the system. This makes the binder type and amount important factors to consider when designing a pyrotechnics composition. Other factors include processing requirements and processing aids both of which may be incompatible with the fuel or oxidiser. Other than directly influencing

the reaction and providing increased cohesion between particles, binders also protect the fuel against premature oxidation (Agrawal, 2010).

Table 3. Effect of binder type on the ignition temperature of a mixture[#] (adapted from BariSin and BatiniC-Haberle, 1994).

Binder	Ignition temperature (K)
Phenol-formaldehyde resin	578
Shellac	575
Fluorel	610
Ethylcellulose	610
Nitrocellulose	618
Polyvinylchloride	595

[#] Al: 35 wt.%; aluminium; $KClO_4$: 40 wt.%; $Ba(NO_3)_2$: 20 wt.%; binder: 5 wt.%

2.1.2.6 Mixing

Homogeneous pyrotechnic mixtures are required in order to ensure reproducibility and high reaction rates (Berger, 2005). An end product with the same mechanical and combustion properties throughout its bulk can be created by breaking down all agglomerates and distributing the components of the mixture evenly (Teipel, 2005). The point where homogeneity is reached can be determined by monitoring the rheological properties or characterising the cured product (Teipel, 2005).

The mixing of the fuel and oxidiser is the most dangerous part of the pyrotechnic production process (Conkling, 1985). Mixing takes place in a variety of forms. Two examples of mixing methods for particles are brushing though screens and tumbling (Conkling, 1985). Polymer extrusion techniques have also been applied in the production of MTV systems to provide a homogenous continuous mixture of components (Koch, 2012). Each of these methods will have its own set precautions and safety measures to ensure safe operation. The mixing technique used is dependent on various factors. These include the stability of the components and the material properties of the constituent components.

2.2 Polymer processing

Compounding requires the homogenous mixing of two or more materials of which one forms the matrix in which the other elements are distributed (Osswald, 2011). The Mueller process is used to continuously produce MTV compositions. The process first wets the magnesium and Teflon with ethanol before it is introduced to Viton which is dissolved in acetone (Koch, 2012). In this process Viton is dissolved and both the magnesium and Teflon remain in the solid phase. The solvent level in this process is important as it affects the viscosity which will then affect the degree to which the additives are distributed (Osswald, 2011). This process employs a twin screw extruder which has the advantage of requiring low solvent levels and the absence of dead spots during homogenization (Koch, 2012).

2.2.1 Mixing polymers and additives

Mixing is of critical importance when trying obtain reproducible results. Highly filled energetic materials exhibit a high melt viscosity. Therefore mixing by turbulence and eddy diffusion does not take place. Another factor to consider is the effect of the fuel size on the processability of the polymer. It is well known that nano-sized fuels provide improved performance it does however greatly increase the difficulty of processing the polymer with traditional mixing methods (Huong et al., 2014). Mixing can be split into two categories namely distributive and dispersive mixing (Dombe et al., 2015).

2.2.1.1 Distributive mixing

Distributive mixing or laminar mixing distributes miscible fluids or particles within a matrix. This distribution is achieved by imposing large strains on the system which leads to increases in the interfacial area (Osswald, 2011). Since the fuels in this case are immiscible solids this mixing mechanism will not be of importance.

2.2.1.2 Dispersive mixing

This mechanism breaks up immiscible fluid droplets or particle agglomerates and distributes them throughout the polymer matrix (Osswald, 2011). The breakup of particle agglomerates are explained by using a simplified case illustrated in Figure 4 where the ideal case is shown using only two spherical particles.

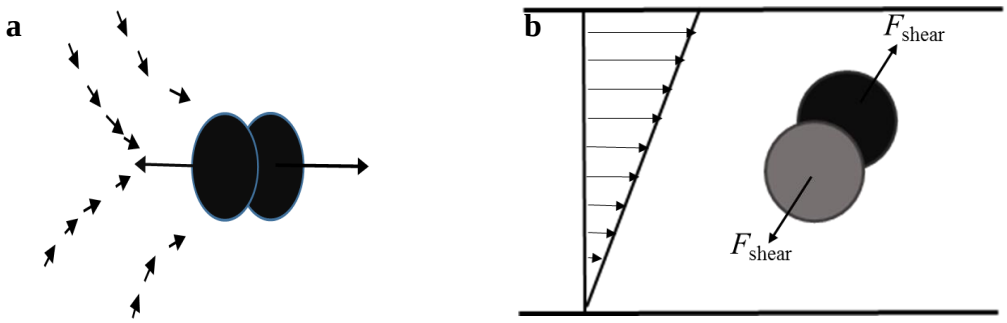

Figure 4. Elongational and shear forces applied to two particle agglomertes during flow (Osswald, 2011).

Figure 4 (a) illustrates the effect of both elongational flow and (b) shear flow patterns. The force required to separate the particles will vary depending on the relative orientations. The maximum shear force will be in effect when the particles are orientated at a 45° angle while the elongational force will be at a maximum at 0° (Osswald, 2011). The magnitude of the maximum separation forces applied to separate the particles are given by equation 3 and equation 4 (Osswald, 2011).

$$F_{elong} = 6\pi\eta\dot{\varepsilon}r^2 \tag{3}$$

$$F_{shear} = 3\pi\eta\dot{\gamma}r^2 \tag{4}$$

In both equations η is the viscosity of the carrier fluid. In this case the polymer melt or dissolved polymer. The magnitude of the strain rate tensor between the two particle radii is depicted by $\dot{\gamma}$. Should the values of shear and elongational flow be the same, then it is easy to show that the maximum elongational force is double that of the shear force. This calculation shows that elongational flow is preferred when mixing and breakup of agglomerated particles is required (Osswald, 2011). The flow type can be determined by calculating the flow number (λ) as illustrated in equation 5 (Osswald, 2011).

$$\lambda = \frac{\dot{\gamma}}{\dot{\gamma}+\omega} \tag{5}$$

In equation 5, $\dot{\gamma}$ is the magnitude of the rate of deformation tensor, while ω is the magnitude of the vorticity tensor. A flow number of zero indicates pure rotational flow, while 0.5 represents simple shear flow and 1 is representative of elongational flows.

There are various mixers that can provide one or more of the mixing types mentioned. These include, Banbury mixers, static mixers, extruders and two roll mills to name a few. Banbury mixers are one of the most common internal batch mixers (Osswald, 2011). It utilises complex shear and elongational flows to break up particulate agglomerates within polymer matrices (Osswald, 2011). Static mixers provide continuous mixing unlike the batch mixing described for the Banbury mixer. Mixing is achieved by pumping the fluid through the mixer housing in which various mixing elements are placed. These elements rotate and divide the flowing polymer. In initial stages of mixing this leads to visible striations within the compound. As the compound progresses through the mixer the interfacial area increases leading to a decrease in striation thickness. The deformation process described utilises shear force instead of elongational forces in order to achieve homogeneity (Osswald, 2011). As is the case with single screw extruders this shear deformation instead of elongation deformational is considered a drawback (Osswald, 2011).

The ideal mixing implement should be able to produce a homogeneous compound with little to no risk of ignition. Several compositional factors will play a role in the processing parameters that are to be used, such as temperature and shear sensitivity. This may also exclude certain equipment types due to incompatibility with the compositions.

2.2.2 Extruders

Twin screw extruders are potentially the most popular continuous mixing devices for a variety of processes (Osswald, 2011). Continuous processing of energetic materials usually employs twin screw extruders (Dombe et al., 2015). Twin screw extruders are used because of the homogenous mixing they provide at reduced friction (Dombe et al., 2015). Co-rotating intermeshing twin screw extruders are used because the pressure is distributed evenly across the periphery, it provides a uniform residence time as well as reduced sensitivity to head pressure reducing the risk involved with the process (Dombe et al., 2015).

The twin screw extruder consists of a barrel with two screws in it. Twin screw extruders are either co-rotating or counter-rotating and either intermeshing or non-intermeshing (Osswald, 2011). Co-rotating systems are known for high pumping efficiency due to the double transport action of the screws (Osswald, 2011). Counter-rotating extruders are known for generating high stresses within the melt due to the calendering action between the screws (Osswald, 2011). It does however also induce high temperature pulses limiting its use for certain applications (Osswald, 2011). The configurations are illustrated in Figure 5.

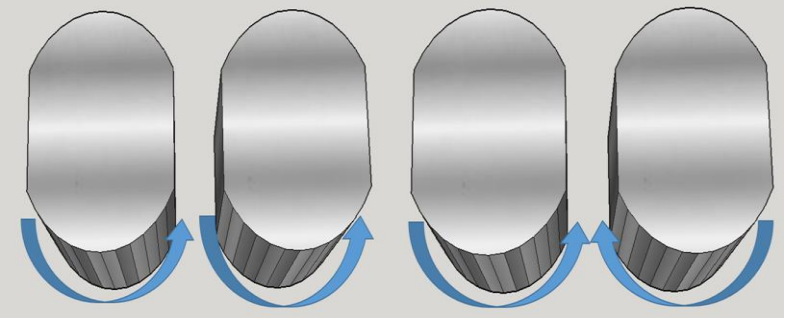

Figure 5. Twin screw extruder configurations, (left) co-rotating and (right) counter-rotating (Osswald, 2011).

The gap between the screw and barrel is important for both transport and safety aspects. For safety reasons, this gap should be 2-3 times larger than the largest particles when processing energetic material containing particulate matter (Dombe et al., 2015). This space is necessary in order to reduce friction, as it may lead to ignition of the composition being processed.

The screw can be divided into different section, each having a different function. These include feeding, melting, mixing, metering and pressure generation required for extrusion (Dombe et al., 2015). These sections will differ in appearance as they are adapted to different roles as shown in Figure 6.

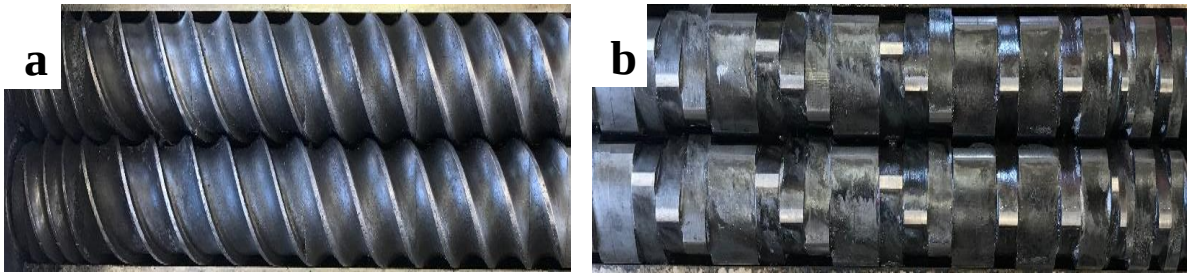

Figure 6. (a) Conveying element, (b) kneading element.

Mixing takes place during the melting and pumping of the polymer. The conveying elements as indicated in Figure 6 (a) are responsible for distributive mixing while the kneading elements in as indicated by Figure 6 (b) provide dispersive mixing (Dombe et al., 2015). Kneading blocks provide dispersive mixing by the intense shear generated by rotation. The melt is pumped through an extrusion die which determines the shape of the final product. A variety of shapes can be extruded such as films, strands and tubes (Osswald, 2011).

The extrusion of the energetic composition requires the monitoring and control of several aspects in order to proceed in a safe manner. These include temperature control, torque control, static electricity and mechanical construction (Dombe et al., 2015). Hot spot formation may lead to disastrous effects. Hot spots may form due to viscous dissipation. This is caused by the shearing of the material inside the extruder and die (Dombe et al., 2015). As demonstrated earlier, shear force is a function of viscosity which in turn is temperature dependent. Therefore close control of the temperature may ensure that the viscosity remains in a suitable range for mixing without leading to excessive heat build-up. Pressure control within the extruder is also of importance. Pressure build up may lead to intra-granular shear or material leaving the barrel through seals, both of which can lead to accidents (Dombe et al., 2015). Torque control systems and explosion proof fittings as well as use of non-spark materials are all systems that assist in maintaining safe operating conditions (Dombe et al., 2015).

2.2.3 FDM

FDM systems deposit a polymer melt layer by layer in order to construct a 3D object(Priedeman, 2011). The melt is extruded through a printing head which moves in the X-Y plane. The extruded melt is deposited on previously deposited layers. The print head repositions along the Z-axis incrementally to place subsequent layers of material (Priedeman, 2011). Each newly deposited layer fuses to the underlying layer as it cools. Head movement is controlled by computer software that slices the CAD model into horizontal layers (Priedeman, 2011) and assigns the coordinates that the head traces depositing layers of material as it moves along (Priedeman, 2011).

2.3. Porous silicon

Porous silicon (PSi) has been investigated for use in pyrotechnics for its nanostructured properties while still being in the micrometer or larger scale. This allows for the application of a relatively inexpensive fuel to a wider range of potential market applications. The discovery of the explosive properties of nano porous silicon (nPSi) was made in 2001 even though the high reactivity of porous silicon was well known by 1992 (Koch and Clément, 2007). PSi wafers and powders have been investigated for pyrotechnic applications. This is due to the significant increases in active surface area that these materials display. By increasing surface areas of micron sized powders one can increase the reactivity of the compound without the problems associated with nano scale materials. Nano scale materials require different processing techniques than those employed for the production of compositions consisting of micron ranged constituents. This is due to the agglomeration inherent with the use of nano-particulates, as well as increased sensitivity of many of the compositions. For this reason increases in surface without producing individual nanometer sized particles can reduce processing technicalities due to the possibility of using more traditional compounding and assembly techniques.

2.3.1 Production

PSi production is based on hydrofluoric acid (HF) etching. Some of the most widely used procedures are electrochemical etching or stain etching with the addition of nitric acid (HNO_3) (Prokes, 1996). Hydrofluoric acid is used in the microelectronics industry for the removal of

silicon dioxide from the surface of silicon wafers (Trucks et al., 1990). Uhlir and Turner first reported the presence of pore formation during electrochemical etching (Searson et al., 1992). This is of great interest since the increased surface area leads to an significant increase in oxidation rates (Clément et al., 2005). These layers are constructed from nanocrystals with large internal surface areas (Clément et al., 2005).

The production of PSi by hydrofluoric acid etching may lead to hydrogen passivation of the silicon surface (Prokes, 1996). This layer of Si-H bonds forms a protective barrier to oxidation under ambient conditions. This preserves the active fuel content of the silicon. Silicon passivated with hydrogen is organophilic (Clément et al., 2005). This leaves the surface hydrophobic. The hydrophobic surface makes the silicon resist oxidation in humid environments (Subramanian et al., 2008).

The complete removal of oxygen from the silicon surface is unlikely (Prokes, 1996). This is because the passivation layer is still oxidised albeit at a slower rate. This aging process takes place over several years (Koch and Clément, 2007). During natural aging a single layer of oxygen atoms is back-bonded onto the silicon surface (Koch and Clément, 2007).

Annealing at lower temperatures allows for the back bonding of oxygen which further stabilises the silicon for storage without noticeably affecting reactivity (Clément et al., 2005) (Subramanian et al., 2008). This annealing proses should remain at low temperature to avoid directly bonding the oxygen to the silicon surface as this would lead to hydrophilic behaviour (Clément et al., 2005).

The annealing process can be used in order to tune the gas produced by combustion with certain oxidisers. This was shown by conducting pressure measurements in a pressure bomb by Churaman et al (2010). Annealed- and as prepared PSi samples were impregnated with sodium perchlorate ($NaClO_4$). It was determined that the gas produced per active gram for the as prepared sample was 0.0129 $mol \cdot g^{-1}$ while the annealed sample produced only 0.004 $mol \cdot g^{-1}$ (Churaman et al., 2010). This change in gas output is thought to be due to the partial removal of hydrogen from the surface that occurs during annealing (Churaman et al., 2010).

This may potentially allow for the same fuel oxidiser combination to be used for a variety of applications where different levels of gas production is allowed. The removal of the oxide layer from the silicon surface is a multi-stage event. The silicon surface is initially covered in fluorine after the removal of the oxide, the fluorine is then replaced by hydrogen as is summarised in Figure 7.

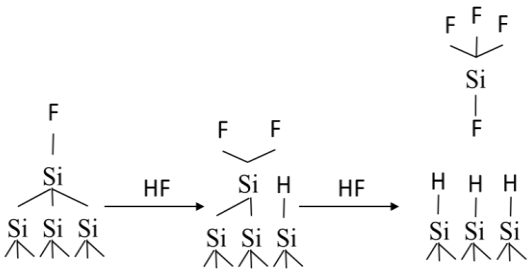

Figure 7. Fluorine replacement by hydrogen on the silicon surface (adapted from Trucks et al., 1990).

The hydrogen passivated surface is unexpected since the Si-F bond has a greater strength than the Si-H bond (Sailor, 2012). The removal of fluorine from the surface of the silicon is due to the high reactivity of the Si-F bond (Sailor, 2012). The instability and thereby reactivity of the Si-F bond is brought on by its highly polar nature (Kolasinski, 2009). Fluorine is the most electron negative element which causes polarisation the silicon back bonds (Kolasinski, 2009). This bond polarisation leaves the silicon surface vulnerable to nucleophilic attack (Sailor, 2012), resulting in its removal and the formation of the Si-H surface coverage. The reaction between silicon and hydrofluoric acid is illustrated by Scheme I, while the silicon dioxide reaction with hydrofluoric acid is illustrated by Scheme II.

Scheme I: $Si+4HF \rightarrow SiF_4+2H_2$

Scheme II: $SiO_2+6HF \rightarrow H_2SiF_6+2H_2O$

The dissolution of silicon in aqueous hydrofluoric acid is slow. This is due to the passivation of the surface by the Si-H bond (Sailor, 2012). For this reason various methods have been developed in order to accelerate the etching, these include electrochemical etching as well as the addition of strong oxidising agent e.g. nitric acid in the etching solution (Sailor, 2012). The addition of oxidisers allows for the etching to commence at a faster rate due to the greater availability of silicon dioxide. Hydrofluoric acid will be able to attack silicon dioxide instead of silicon.

2.3.1.1 Wafer etching

The removal of the oxide layer from silicon wafers by hydrofluoric acid etching is well known. Various techniques have been developed of which only the electrochemical route will be discussed here. The surface morphology of the wafer can be tailored to fit the application. The surface finish ranges from porous to polished. In this case porosification of the silicon is required. The process can produce nano- to micro-meter sized pores depending on the conditions (Plummer et al., 2011).

Electrochemical etching requires two electrodes an anode and a cathode. When placed in the electrolyte the electrodes maintain charge neutrality and complete the circuit (Sailor, 2012). The electrolyte usually consists of hydrofluoric acid and ethanol (du Plessis, 2014). A simple example of an etching setup is illustrated in Figure 8. In this configuration silicon is the anode. This implies that an oxidation reaction is taking place at its surface. The general reaction mechanisms at both electrodes are illustrated in Figure 8, valence band holes (h^+) are also depicted.

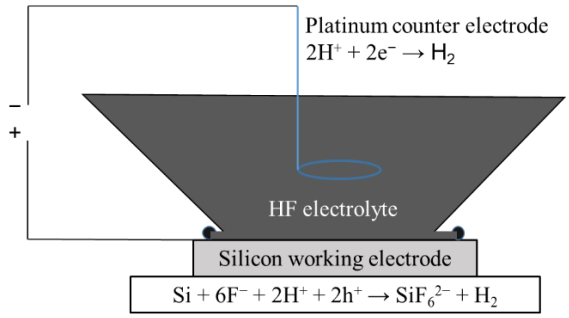

Figure 8. Electrochemical cell used for production of PSi (Sailor, 2012).

The porosification process shown in Figure 8 has various variables that affect the formation of pores. The concentration of hydrofluoric acid, etching times and doping levels will all affect the depth and size of the pores formed during etching if the potential across the cell is kept constant (Clément et al., 2005). Alternatively the etching process can be switched from polishing to porosification by changing the cell potential as illustrated in Figure 9.

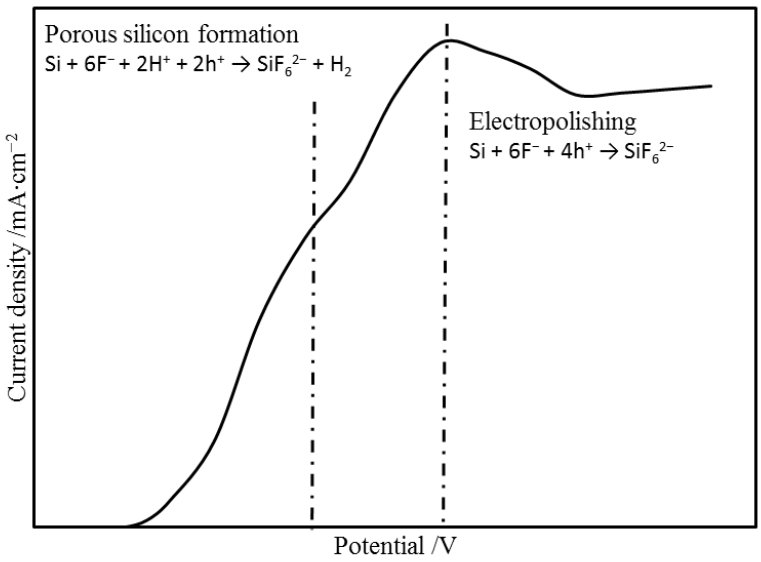

Figure 9. Current density as a function of applied potential (Sailor, 2012).

Three regions are indicated in Figure 9, the two extremes being the porosification region and the electropolishing region these are separated by a transitional region. Acid concentration plays a role in the shape of the curve. High hydrofluoric acid concentrations paired with low current densities favour PSi formation while the reverse is true for polishing (Zhang et al., 1989). This trend holds for all of the Si wafer types, p^-, p^+, n^+, n (Zhang et al., 1989).

Porous silicon wafers require a very large specific surface area to find use in pyrotechnics (du Plessis, 2008). As mentioned, increasing concentrations as well as etching times can assist with this. It has however been found that the porous layer loses its mechanical stability should the etching time be extended beyond a certain point (Clément et al., 2005). It should also be kept in mind that, beyond a certain point, the specific surface area decreases with an increase in pore size and overall porosity (du Plessis, 2008). This means that producing very large specific surface areas may lead to problems with pore loadings as the oxidiser may not be able to penetrate into the porous layers (du Plessis, 2008). The implication is that an optimum pore size exists that will allow for efficient loading of oxidisers as well as provide the increased surface area required (du Plessis, 2008). The highest energy yields are achieved when the pores allow a stoichiometric amount of oxidiser to be loaded (du Plessis, 2014). This will provide the fuel with enough oxidant to react to completion. A study using sodium perchlorate monohydrate ($NaClO_4 \cdot H_2O$), sulfur (S) and gadolinium(III)nitrate hexahydrate

($Gd(NO_3)_3 \cdot 6H_2O$) as oxidisers found this optimum pore size to be in the order of 3 nm (du Plessis, 2008). This pore size will however differ for different oxidisers as another study found an optimal size of 11.8 nm for aluminium nitrate oxidiser (du Plessis, 2014). Some of the factors controlling the growth of the porous layer are compared in Table 4.

Table 4. Porous layer thickness dependence on current density and etching time (adapted from Clément, et al. (2005)).

Wafer type	Current density (mA/cm^2)	Etching time (min)	Thickness (µm)
p^{++}	43.5	30	70
	43.5	60	138
	60.9	30	90
	60.9	60	170
p^{+}	43.5	30	72
	43.5	60	132
	60.9	30	94
	60.9	60	160

An increase in etching time at constant current densities clearly leads to an increase in the thickness of the porous layer. The same can be said about changing current densities. Clément, et al (2005) found that the maximum attainable porous layer thickness was 200 µm for p^{++} when using standard electrochemical etching.

Clément, et al. (2005) altered the process and were able to obtain thicker a layer thicknes of nearly 500 µm. They adjusted the standard etching technique by starting with higher current densities which would allow larger pore diameters to form, the current density was then decreased with time allowing the etching solution to penetrate the pores. The larger pores combined with breaks in the etching process would assist with the removal of hydrogen gas from the pores as well as equilibration of the the etching solution concentration at the reaction interface (Clément et al., 2005).

Alternatively pores can be created then widened by a two stage process which starts with anodization at low hydrofluoric acid concentrations and low current dencities followed by a open-circuit pore widening stage in dilute hydrofluoric acid (Prokes, 1996).

The pore dimensions will limit the potential oxidants and loadings that can be used. Production of wafers for energetic use requires knowledge of the pore location. For this reason hydrofluoric acid resistant masks with a known pattern of openings are used to cover the wavers (Clément et al., 2005). An example of a suitable mask material is silicon nitride (Si_3N_4) (Clément et al., 2005). These masks allow for the production of wafers with known porous regions that can then be filled with oxidisers.

2.3.1.2 Powder etching

The methods discussed up until this point covered wafers. Etching of powders however require different methods to be used. Various ways have been developed to produce PSi powders. These include scraping the porous layers of wafers, milling of wafers as well as direct etching of silicon powders. Direct etching of powdered silicon is achieved with stain etching. Stain etching has the benefit of being readily scalable to large batches, it is for this reason that it is the main method used for commercial production of PSi powders (Sailor, 2012). In this etching technique the reaction is driven by a chemical oxidant instead of the power cell (Sailor, 2012). Nitric acid is the most widely used oxidant (Sailor, 2012). Varying the nitric acid concentration affects the porosity as illustrated in Table 5.

Table 5. Effect of nitric acid concentration on BET surface area (adapted from Subramanian et al (2008)).

Particle size (μm)	**Nitric acid concentration (%)**	**BET surface area (m^2g^{-1})**
4	2	41
4	3.4	143
11	2	56.3
11	3.4	128

Similar to the wafers increases in surface area are accompanied by decreases in pores size (Subramanian et al., 2008). Once again oxidiser loading will be dependent on the etching condition used to produce the PSi. Stain etching does not allow for the same control provided by electrochemical etching. One reason for this being the size distribution of particles used in the process. Methods for have been developed to improve reproducibility of stain etching processes such as monitoring the photoluminescence of the reaction mixture (Subramanian et al., 2008, Farrell et al., 2006). The production of PSi can be monitored by illuminating the silicon with ultra violet light. The formation of pores is indicative of nanocrystals forming within the larger grains resulting in a bright orange–red emission (Subramanian et al., 2008). Stopping the etching process as soon as luminescence is observed allows for the production of particles with the highest surface area (Subramanian et al., 2008).

Metal-assisted etching has been shown to produce particles with exceptionally high surface areas (Loni et al., 2011). Loni et al (2011) reported a surface area increase from 10 $m^2 \cdot g^{-1}$ to 480 $m^2 \cdot g^{-1}$ utilising a metal assisted etching technique. In this method a metallurgical grade silicon was etched in a solution consisting of hydrofluoric acid and iron(III) chloride ($FeCl_3$). The metal assisted reaction mechanism is shown in Scheme 3 (Loni et al., 2011).

Scheme III: $Si + Fe^{3+} + 6HF \rightarrow H_2SiF_6 + Fe^{2+}\ 4H^+ + 3e^-$

The ferric ion assists in pore nucleation and penetration into the particle (Loni et al., 2011). This etching process is exothermic. Furthermore several gasses are released during the process. The particles etched in this method are recovered from two different states. During the etching a dense foam is produced which consists of etched silicon particles, while some remain within the etching solution. The particles recovered from the foam have surface areas smaller than those recovered from the etching solution. This is due to the reduced contact time between the particles and the etching solution (Loni et al., 2011). This is potentially problematic as the foam is a hydrophobic substance therefore indicating hydrogen passivation. Since hydrogen passivation is required in order to produce an oxide free fuel the foam should be the target product. When attempting to achieve high surface areas it is important to prolong the contact time between the silicon in the foam and the etching solution.

2.3.1.3 Alternatives

Combustion synthesis followed by chemical treatment can produce nPSi particles. Terry et al (2014) used salt assisted combustion synthesis to produce the base silicon for the chemical treatment process. The combustion synthesis of the silicon proceeded according to Scheme IV (Terry et al., 2014).

Scheme IV: $SiO_2 + 2Mg + \alpha NaCl \rightarrow Si + 2MgO + \alpha NaCl$

The sodium chloride (NaCl) in Scheme IV reduces the combustion temperature ensuring that the produced silicon does not melt thereby maintaining its nanostructure (Terry et al., 2014). The associated value for α is between one and two. Larger values of α lead to a drop in combustion temperature as well as protective layer formation around the silicon thereby further protecting the nanostructure (Terry et al., 2014). Other factors found to affect the combustion synthesis process was the reactor pressure, crucible dimensions and sample geometries (Terry et al., 2014). The factor that was found to affect the morphology the most was the chemical treatment after the combustion synthesis. Terry et al. (2014) used three different treatment methods to achieve different morphologies. Two of the methods consisted of a single treatment while one consisted of two different chemical treatments as summarised in Table 6.

The tabulated results indicate that the post combustion synthesis treatment drastically affects the particle morphology. The size of the nanostructures decreased from method one to three while the amount of agglomeration increased (Terry et al., 2014). No mention was made of hydrogen passivation being observed for any of the methods. Which brings into question the long term stability of the PSi produced in this fashion.

Table 6. Effect of treatment on surface morphology (Terry et al., 2014)

Method	Treatment	Concentration (vol. %)	Time (h)	D_{50} (µm)	B.E.T ($m^2 \cdot g^{-1}$)
1	Hydrochloric acid (HCl)	5	2	4.67	46 ± 5
	Stage 1				
2	Hydrochloric acid	5	2	1.92	25 ± 2
	Stage 2				
	Water	40	3		
	Ethanol (C_2H_5OH)	30			
	Hydrofluoric acid	20			
	Acetic acid ($C_2H_4O_2$)	10			
3	Hydrochloric acid	30	2	23.61	230 ± 5

There are other methods for removal of silicon dioxide. Hydroxide (OH^-) etching is one such method. The reaction between silicon and OH^- is shown by Scheme V (Kolasinski, 2009).

Scheme V: $$SiO_2 + 2H_2O + 2OH^- \rightarrow [SiO_2(OH)_2O_2]^{2-} + 2H_2$$

This method does however not leave the silicon with the hydrogen passivated surface. This means that the silicon will be vulnerable to further oxidation as the oxide layer is stripped off.

2.3.2 Application

However, the use of PSi in pyrotechnic compositions tends to be problematic since the increased surface area can only be utilised if the oxidant is able to penetrate the pores. This limits the number of oxidisers that can benefit from the increased surface area, as pore filling has its difficulties. Due to the size of the pores filling methods are usually solvent based or require the oxidiser to be molten. This makes the application of polymer based oxidisers potentially viable as polymers have relatively low melting points or depending on the polymer solvent methods may be applicable.

3. Material selection

As mentioned the objective is to produce a pyrotechnic composition that is stable enough to undergo melt processing using a fluoropolymer as the oxidiser. This would require fuel oxidiser mixtures that are stable enough to undergo the temperature and shear experienced in an extruder.

3.1 Oxidiser

The choice to use partial or perfluorinated polymer will be driven by various factors. Energetic potential, cost, processing conditions and safety are all factors that should be considered. Important properties for the oxidiser would include:

- high fluorine content;
- melt processability;
- solubility; and
- a safe difference between melting and decomposition temperatures.

A high fluorine content is required due to it being the oxidiser in the system. Partially fluorinated polymers also increase the risk of producing potentially dangerous products such as hydrofluoric acid. PTFE has the highest fluorine content of the fluoropolymers but it is not melt processable. This excludes it from being the continuous phase. Even though the stated goal is to produce a melt processable composition solubility of the polymer is necessary, especially during the initial stages of development. This is due to the unknown stability of the composition. If the polymer is soluble at relatively low temperatures, the composition can be compounded and ignition temperature determined. This is done to determine whether or not the composition will be extrudable. As mentioned earlier the decomposition temperature of the polymer is of critical importance when looking at the ignition temperature of the composition. If the temperature difference between decomposition and melting is small the risk involved may be too great for extrusion. Ignition and decomposition temperatures of several polymers are listed in Table 7.

Table 7. Summary of chemical and physical properties (adapted from Koch 2012)

Name	Formula	Fluorine content (wt.%)	Melting point (°C)	Decomposition temperature (°C)
PTFE	$(C_2F_4)_n$	76	328	>400
PCTFE	$(C_2CLF_3)_n$	48.9	211	>400
PVDF	$(C_2H_2F_2)_n$	59.4	154-184	350
Viton A	$(C_2H_2F_2)_7$ $(C_3F_6)_2$	66	-	>400

3.1.2 Selected polymers

The following resins were selected for the process: FK-800® and Dyneon 31508®. Both were obtained from 3M. Both of these are copolymers of chlorotrifluoroethylene (CTFE) and vinylidene fluoride (VDF). FK-800® consists of 83.7 wt.% CTFE and 16.3 wt% VDF. While Dyneon 31508® consists of 18.6 wt.% CTFE and 81.4 wt.% VDF. A third polymer was selected in order to assist with processing of the other polymers. This was the LFC-1® fluoroelastomer liquid from 3M™. Which is a partially fluorinated compound consisting of poly (vinylidenefluoride-co-hexafluoropropylene).

3.2 Fuel selection

Aluminium and silicon were chosen as fuels for the selected system. Both being widely used in pyrotechnics, are relatively inexpensive and provide the benefit of being more stable than magnesium. The use of a metal and non-metal fuel allows for the opportunity to test the ability of surface modification techniques in improving the combustion performance of the non-metal. Silicon has the potential to even replace aluminium altogether should the resulting surface modification of the silicon prove to be successful and energetically viable. Aluminium powder was provided by Grinman South Africa. The metallurgical grade silicon used was provided by AEL mining services.

3.3 Fire retardant

Magnesium hydroxide was selected for initial compounding, extrusion and printing trials. It was chosen in order to determine operating conditions of the mentioned processes. Magnesium hydroxide is used as a fire retardant in the polymer industry and should therefore provide a safe composition when experimenting with the temperature profiles required for the melt processing procedures. The magnesium hydroxide powder received from Merck was of a lab grade quality.

3.4 Safety considerations

3.4.1 Pyrotechnics

Pyrotechnic compositions as with other energetic materials should be handled with care due to the inherent dangers associated with them. For this reason mixing, testing and storage of compositions takes place in a licensed pyrotechnics laboratory with the following features to mitigate the threat of accidental initiation:

- workspaces are grounded;
- floors are designed to prevent static build up;
- lights and other electrical connections are dust proof; and
- access control as well as safe storage for compositions.

Personal protective equipment included leather gloves, conductive shoes, lab coats, eye and respiratory protection.

3.4.2 Hydrofluoric acid

Special mention should be made about precautions taken when using hydrofluoric acid. Use of hydrofluoric acid was limited to a specifically designated laboratory which was supplied with all of the appropriate protective equipment and emergency equipment to deal with spills or exposure. Acid handling was only done when wearing impervious gloves. Experiments were conducted in a fume hood to limit exposure to vapour. Calcium gluconate gel was kept on hand in case of skin contact. Acid waste was neutralised using calcium carbonate ($CaCO_3$).

4. Experimental methods

4.1 Thermodynamic simulation

Simulations were done in order to determine the optimal fuel loading under adiabatic conditions. Simulations were run under the same conditions that the composition would experience in the bomb calorimeter. This required the addition of the inert gas helium (He) to the system while confining it to a volume of 240 mL. The software used to calculate the thermodynamic potential of the system was EKVI Calc 4.3. Simulations were done by maintaining a constant oxidant mass while incrementally increasing the fuel mass. The fuel was varied from 5 wt.% to 75 wt.% of the composition.

4.2 Characterisation

Fuels were received as powders and were characterised before and after modifications, if any were made. Polymers were received as powders, pellets and waxes.

4.2.1 Particle size distribution

Particle sizing of the fuels was done using a Malvern Mastersizer Hydrosizer 2000. The Mastersizer uses dynamic light scattering to determine the particle size distribution. Water was used as the dispersant. Where necessary, surfactants were used to break down agglomerates.The water was continuously stirred in conjunction with ultrasonic agitation, for the duration of tests. Each sample was run ten times and results were averaged in order to obtain the particle size distribution.

4.2.2 Surface area

The specific surface area of the fuels were analysed using Brunauer-Emmett-Teller (BET) theory, with a Micrometrics Tristarr II machine. Nitrogen was used as the probing gas. Degassing of all samples was done at a temperature of 100°C for a period of 8 hours. Degassing took place in the Micrometrics VacPrep 061 Sample Degas System. The software used to perform the analysis was, Tristar II 3020.

4.2.3 Microscopy

A scanning electron microscope (SEM) was used in order to study the morphology of the starting materials as well as the combustion products. The microscope used for this analysis was a ZEISS Gemini ULTRA Plus field emission SEM at 1.00 kV. Samples were prepped for analysis by coating them five times with carbon at alternating angles. This was done using a SEM auto-coating unit E2500 (Polaron Equipment Ltd) sputter coater.

The modified silicon samples were analysed using transmission electron microscopy (TEM). This was done in order to determine if the treatment succeeded in producing a porous structure. A multi-purpose TEM Philips 301 was used for the analysis. Samples were prepared by sonicating the powder in ethanol in order to break up agglomerates. Thereafter, the suspension was deposited onto a copper disc using a pipette and dried before analysis.

Optical microscopy was done in order to determine the mixing quality obtained. A Leica DM 2500M microscope was used to view the samples. The software used to capture the images was Leica materials workstation version 3.6.1. Samples were prepared as films or cross-sections of extruded filaments.

4.2.4 Composition

Fuel composition was determined before use in further processes. Elemental composition was evaluated using X-ray fluorescence (XRF). Analysis was done using an ARL Perform'X Sequential XRF instrument with Uniquant software. The software can detect all elements between sodium (Na) and uranium (U). The analysis however only reports elements found above the detection limits within the reported range. All samples were prepared as pressed powders.

X-ray diffraction (XRD) analysis was done using a Bruker D8 Advance diffractometer with a 2.2 kW Cu Kα radiation (λ=1.5406 nm) fitted with a LynxEye detector with a 3.7º active area. Scans were done in reflection mode in the angular range 5° to 90° 2θ.

4.2.5 Thermal analysis

Thermogravimetric (TGA) analysis was performed using a Hitachi STA7300 Thermal Analysis System. The samples were weighed and placed in alumina crucibles for analysis. Samples were heated at rate of $10°C \cdot min^{-1}$ from ambient temperature to a temperature of 600°C. Analysis was performed in a nitrogen atmosphere.

4.2.6 Rheology

Rheological studies were done on the oxidisers used. These measurements were made at the Council for Scientific and Industrial Research (CSIR). The instrument was a SmartRheo capillary rheometer. A type 8.09 PT piston was utilised. The capillary diameter was 1 mm and the L/D ratio was 5. All measurements were made at 230°C.

4.3 Treatment

The silicon powder was treated chemically in order to increase the specific surface area without drastically reducing the particle size. This chemical treatment consisted of a two stage chemical etching process. The first stage was a potassium hydroxide etch which lasted 24 h. The silicon was recovered by centrifugation. After three distilled water washes the powder was dried with the assistance of acetone. The dried silicon was then contacted with a hydrofluoric acid solution. This step lasted for one hour after which the silicon was recovered by centrifugation. The silicon was washed three times with distilled water. Followed by a methanol wash.

This two staged procedure was compared to silicon prepared according to the method outlined in (Farrell et al., 2006). The method used nitric acid as an oxidiser during the hydrofluoric acid etching stage. Sample recovery proceeded as discussed above. After the final wash the silicon is dried under vacuum. A summary of the etching procedure is illustrated in Table 8

Table 8. Etching conditions.

Treatment	Silicon mass (g)	Concentration of etchant (M)	Volume (L)	Etching time (hr)
Two stage etching process				
KOH	250	0.47	2.5 L	24
HF	50	6.5	0.170	1
Single stage etching process				
HF	30	10	0.1	1
HNO_3		3.56		

4.4 Compounding and extruding

Initial compounding was done using solvent methods. Batches of 100 g were prepared from polymer and selected fillers. A 10 wt.% solution was made consisting of polymer and an appropriate solvent. To this solution the inert compound or fuel was added to have achieve the target additive loading. The additives were dispersed throughout the dissolved polymer by continuously stirring the mixture for an hour. After which the polymer additive mixture was precipitated out of solution by slowly adding the solution to a water bath. The recovered polymer was then dried in an oven to remove water and any last traces of solvent. Once dried it was shredded. A lab-scale single screw extruder was used to produce a filament of controlled diameter. Diameter control was achieved with online diameter measurements and tension controller. The specifications of the extruder used are summarised in Table 9.

Table 9. Extruder specifications.

Property	Value
Barrel internal diameter (mm)	17.8
L/D	23:1
Max. linear draw speed ($cm \cdot s^{-1}$)	18.1
Max. temperature at die (°C)	400

The compositions were only added to the extruder after steady operation was achieved with acrylonitrile butadiene styrene (ABS). This allowed for less wastage of material during start-up. Once a constant filament diameter was achieved the composition was added. This was then followed again by ABS to completely remove the sample from the extruder. Cleaning was achieved by passing low-density polyethylene (LDPE) through the extruder thereafter.

Alternatively a co-rotating twin-screw extruder was used in order to improve the mixing of the system. The extruder was a Thermo Scientific™ Process 11 parallel twin-screw extruder. Diameter control on this extruder was less accurate as there was no online method of measurement. This meant that filament diameters had to be measured by hand at regular intervals. Adjustments were made to drawing speed based on the measurements made. The specifications of which are summarised in Table 10.

Table 10. Twin-screw extruder specifications.

Property	**Value**
Barrel internal diameter (mm)	11
L/D	40
Throughput ($g \cdot h^{-1}$)	20-2500
Max. temperature at die (°C)	350

A solventless compounding method was chosen for samples processed by the twin screw extruder. Due to the LFC-1® having a wax like consistency it was mixed with the aluminium using a roller. The aluminium was rolled into the LFC-1®. After which the chosen oxidiser was added and thoroughly mixed. The mixture was then put through several shredding cycles in order to break down and distribute the components as evenly as possible. These compositions were then ready to be extruded.

4.5 Printing

Pyrotechnic compositions were only printed after testing was done using the inert filler compound. A FDM-type 3D printer was used to print both the inert composition as well as the actual composition. The printer used was a PrinRbot Simple Model 1403. It had a direct drive extruder for a filament diameter of 1.75 mm. A heated bed was used in order to assist with adhesion of the polymer to the printing bed and to lower warpage problems due to the relatively high printing temperature that was used. Printing was done at a temperature of 230°C. Preliminary prints were simple rings or cubes all with solid infill.

4.6 Energetic properties testing

4.6.1 Differential thermal analysis (DTA)

The analysis was done using a Shimadzu DTA-50. Sample sizes were approximately 15 mg to 20 mg with an equal mass of standard, aluminium oxide (Al_2O_3) used. Alumina pans were used to house the sample as well as the standard in the furnace during each run. A heating rate of 50 °C·min^{-1} was used to reach a maximum temperature of 1000 °C. An inert gas, argon (Ar) was provided at a flow rate 20 ml·min^{-1}. The DTA was used in order to estimate the onset temperatures of phase changes as well as that of the pyrotechnic reaction. This was necessary in order to determine the viability of melt processing the composition. Raw materials were analysed before compositions were analysed in order to determine which phase change would most likely trigger ignition.

4.6.2 Open air burn tests, laser ignition and burn rate

Compositions were first burnt in open air before further testing was done in order to establish viability of the compositions. These tests were done by contacting the samples with a butane torch. Burn temperatures were measured using both an infrared (IR) camera and a pyrometer. The pyrometer was a Raytek model RAYMM1HVF1L. The software used for analysing the pyrometer signal was DataTemp® multidrop. Both of these systems were necessary due to the infrared camera having an upper temperature limit of about 700°C and the pyrometer had a lower limit of roughly 500°C.

Burn rates were measured using infrared video footage of burn tests. The camera used was a Pyroview 380L compact infrared camera. It was positioned side on to the composition. The camera had an acquisition frequency of 50 Hz. The data acquired was analysed with Pyrosoft Professional version 2.15.1 software. Samples were cut to be 105 mm long. Measurements were made on the last 57 mm of the sample. This was done in order to measure only the rate of the fully formed flame front as it proceeds along the sample. Samples were placed 300 mm away from the camera within a rectangular groove cut into a pyrophyllite block. The groove was 4 mm wide and 2 mm deep. An alumina tile was used to cover the groove if partially enclosed systems were necessary. Ignition was achieved by contacting the samples with a butane torch.

Time to ignition was determined by using infrared video footage obtained during laser ignition trials. A Synrad model 48-2 carbon dioxide (CO_2) laser was used for these tests. The beam had a wavelength of 10.6 μm focussed to a point of 1.72 mm. The laser had a maximum power output rating of 27 W. Samples were mounted in an upright position so that the beam could strike the sample on the flat top surface. The power output for the laser ranged from 2 W to 10 W for these tests. IR imaging was used to monitor the point of contact in order to determine the time to ignition. This was done by using the point in time at which the sample was illuminated by the laser. Once ignition was achieved the sample would produce its own IR signature. With these two points known the time to ignition could be calculated with equation 6 using the number of frames that had captured (Δframes). With the time to ignition known the maximum energy potentially absorbed (E) by the sample could be calculated using the power setting (P) with equation 7.

$$\Delta t = \Delta\text{frames} \times 50^{-1} \tag{6}$$

$$E = P \times \Delta t \tag{7}$$

5. Material preparation and characterisation

5.1 Aluminium

The aluminium powder was brushed through a screen with 25 µm openings. Sieved aluminium was analysed using XRD and XRF. The results of which are summarised in Table 11 and Figure **10**.

Table 11. XRF analysis of aluminium powder.

Element	Al	Mg	Si	Fe	Mn	Na	V
wt.%	99.33	0.22	0.22	0.13	0.03	0.03	0.01

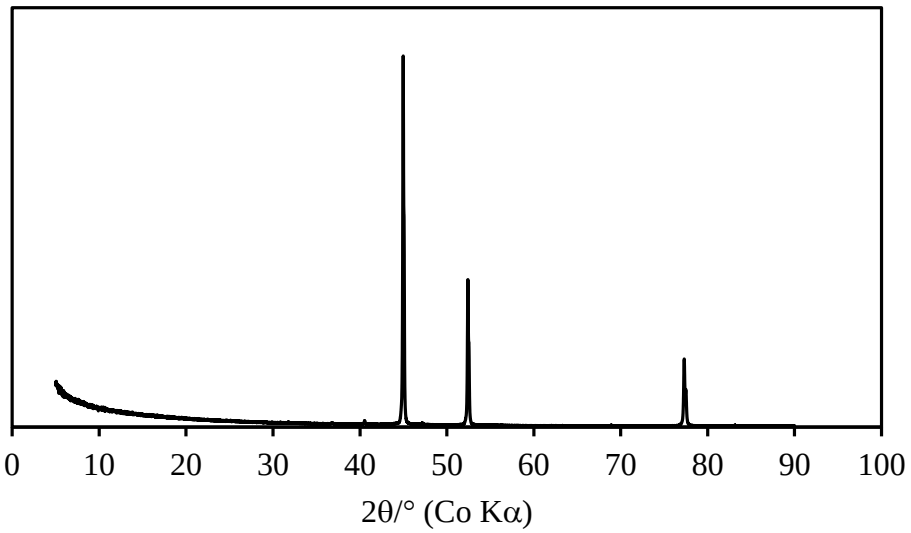

Figure 10. XRD diffractogram of the aluminium powder.

XRF and XRD analysis indicate that the aluminium contained only trace impurities. The particle size distribution and BET surface area, post sieving, are summarised in Table 12 and illustrated Figure 11.

Table 12. Aluminium size and surface area.

D_{10} (µm)	D_{50} (µm)	D_{90} (µm)	BET surface area ($m^2 \cdot g^{-1}$)
4.47	10.7	23.2	2.4

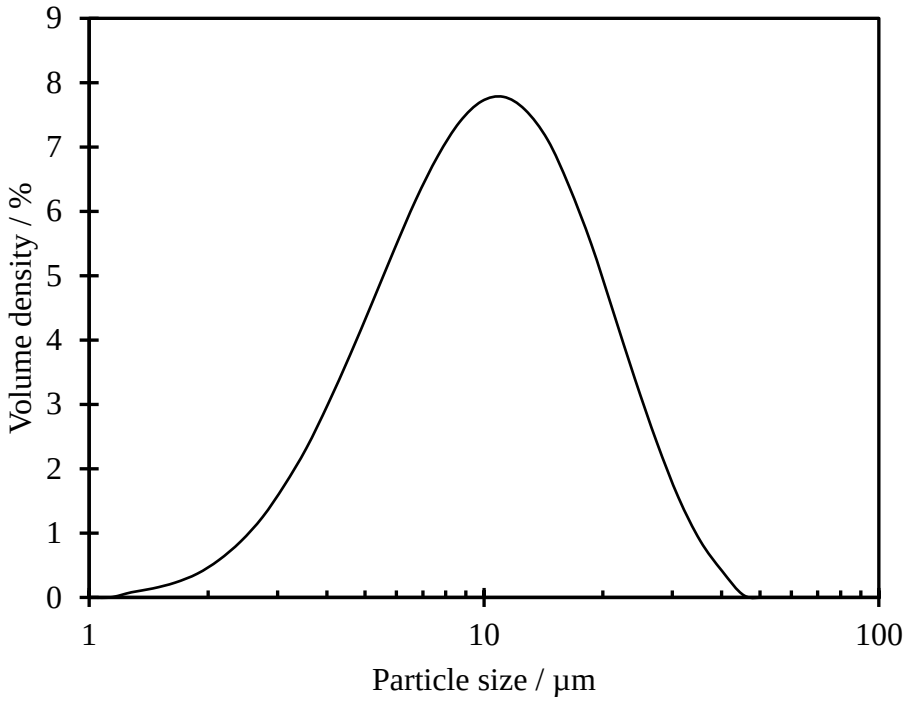

Figure 11. Aluminium particle size distribution.

The results in Table 12 show that the process of sieving the aluminium was successful in removing larger particles as the D_{90} is smaller than 25 µm. However from Figure 11 it was clear that there was a fraction of particles larger than 25 µm. This was attributed to agglomeration.

5.2 Silicon

A metallurgical grade silicon was obtained and used for this process. XRD and XRF analysis was done on the silicon powder. The results of which are shown in Table 13 and Figure 12.

Table 13. Major components as picked up by XRF analysis of silicon powder.

Element	Si	Fe	Al	Ca	Mg	Ba
wt.%	98.08	0.82	0.34	0.33	0.09	0.08

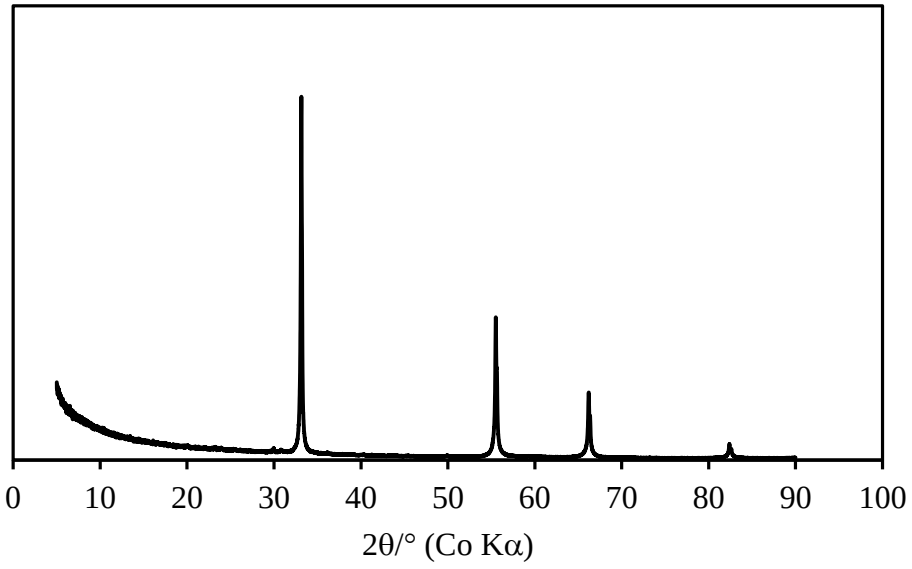

Figure 12. XRD analysis of silicon powder.

The XRD and XRF results indicated that the silicon was relatively pure. The morphology of the silicon used changed throughout the course of treatment. Treatment 1 refers to the two stage etching process while Treatment 2 refers to the single stage process. The results of the surface treatments are shown in Table 14 as well as Figure 13.

Table 14. The effect of surface treatment on the silicon particle dimensions.

Sample	D_{10} (µm)	D_{50} (µm)	D_{90} (µm)	BET surface area ($m^2 \cdot g^{-1}$)
Neat	0.70	2.1	8.54	9.7
Treatment 1	11.05	140.5	386.7	93.9
Treatment 2	0.67	2.60	74.16	13.5

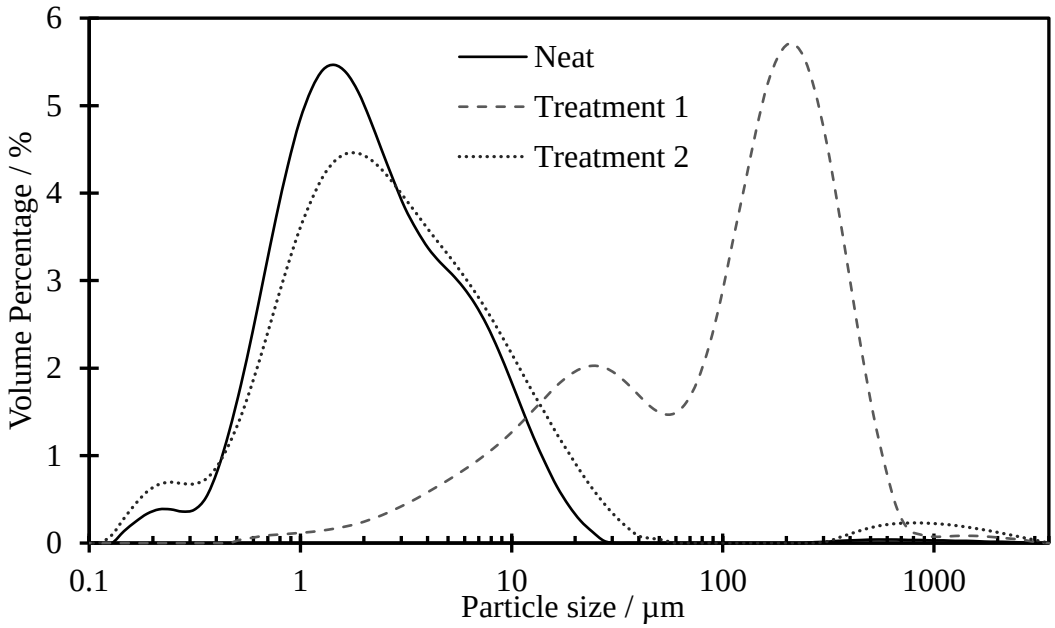

Figure 13. Shift in silicon particle size distribution due to surface treatment.

Table 14 shows a clear difference in post treatment particle sizes. With a shift to larger particles being the trend for both treatment types. The reason for the shift in measured particle size was thought to be due to agglomeration as the drastic increase in surface area especially in the case of the two stage process could only be obtainable through a significant decrease in particle size or a high level of porosification. This is supported by the double peaked nature of the distributions as illustrated in Figure 13. Further evidence of this agglomeration was obtained by SEM imaging as shown in Figure 14.

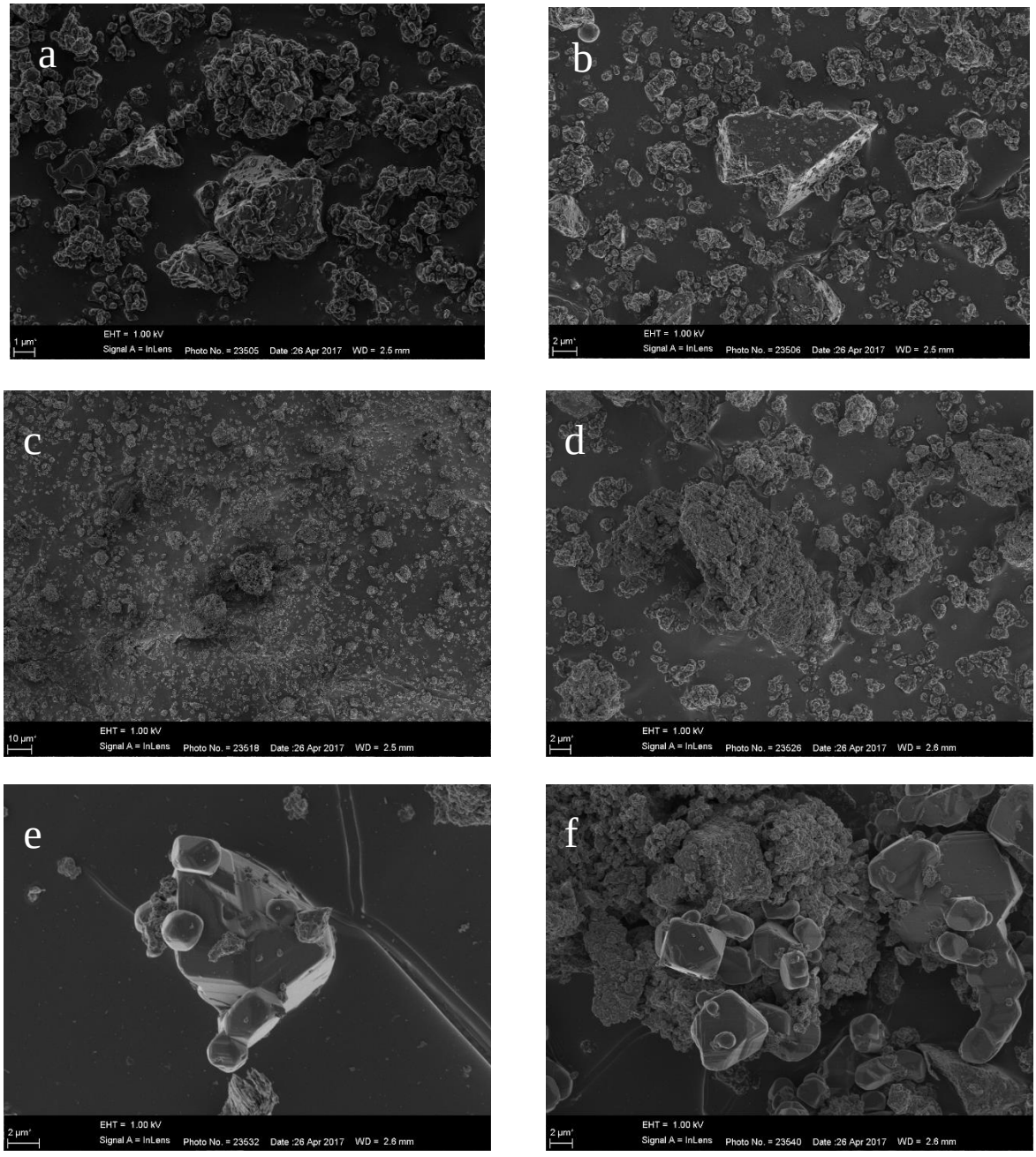

Figure 14. SEM images showing silicon at different stages during processing. (a-b) Silicon before any treatment; (c-d) Silicon after potassium hydroxide etch; (e-f) Silicon after hydrofluoric acid etch.

The SEM images representing the untreated silicon shows particle agglomerates as well as larger particles with somewhat cubic shapes. These cubic particles are covered by agglomerates of smaller jagged particles in the images that represent samples recovered from potassium hydroxide etching. The final row of images illustrate samples recovered after hydrofluoric acid

etching. Cubic particles are once again visible. These are however still covered in smaller particles which can explain the shift seen in the particle sizes. A stepped etching pattern is also visible on these particles showing interaction between the etching solution and the silicon.

TEM analysis was done in order to determine if the porous layer was formed as well as to compare the difference in the final products of the two staged and single staged etching procedures. The results of which are illustrated in Figure 15.

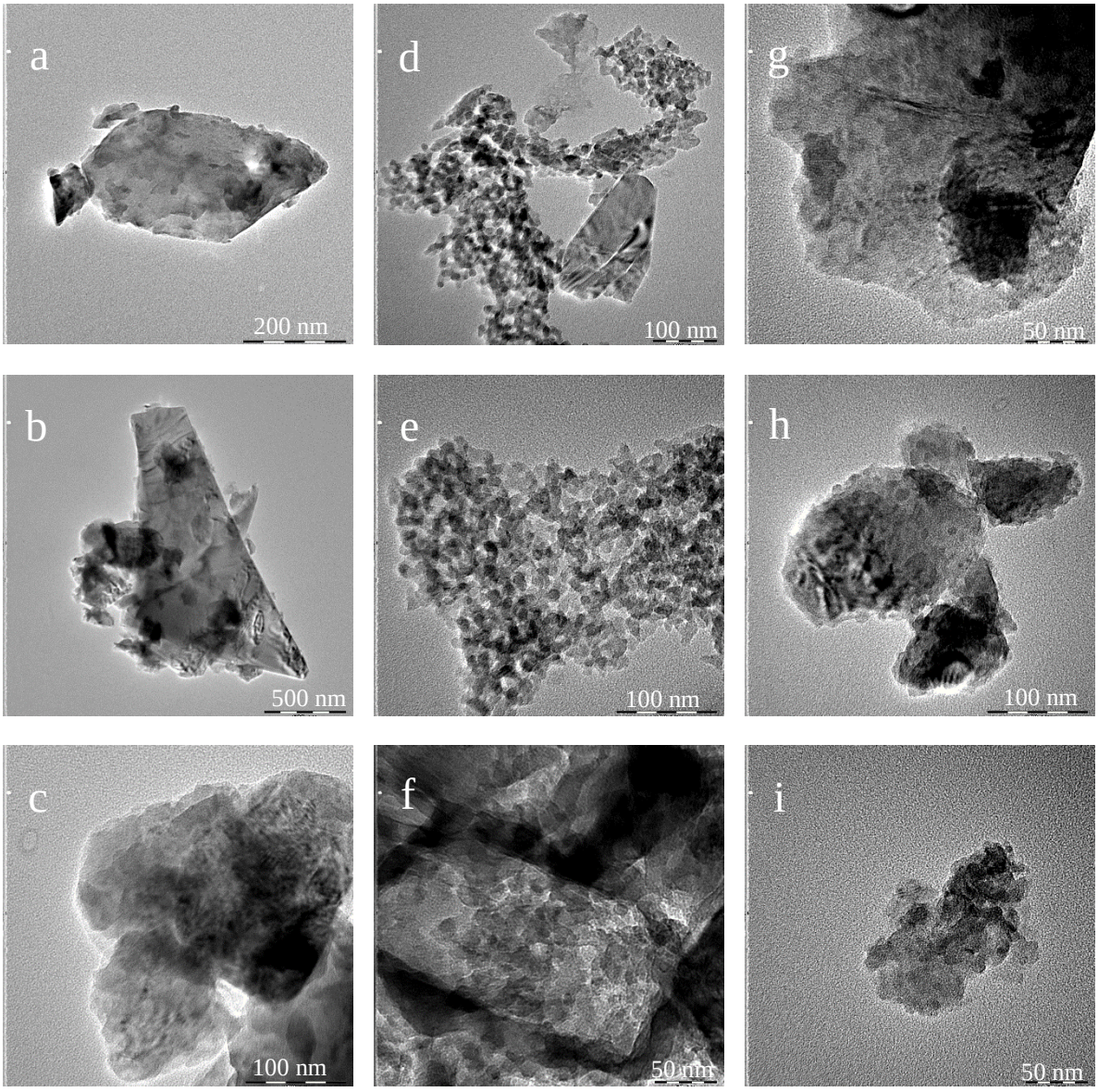

Figure 15. TEM images of (a-c) untreated silicon, (d-f) two stage processed silicon and (g-i) single stage processed silicon.

Figure 15 made it clear that both etching procedures changed the structure of the silicon powder particles. The two stage process as depicted in Figure 15 (d-f) had reduced much of the original structure to smaller particles that are agglomerated around larger particles. This may provide the explanation for the shift in particle size depicted in Figure 13 and the significant increase in BET surface area witnessed. The single stage process yielded larger, less agglomerated, particles compared to the two stage process. Both processes had particles with dimples or shallow pores visible on the surface Figure 15 (f-i). This supports the drastic increase in BET surface area witnessed.

The composition of the particle surfaces was altered by each treatment stage. During the first stage of processing the silicon surface was oxidised, while the second stage of the process removed the oxide layer leaving the silicon with a surface covered with Si-H bonds. This is illustrated by the DRIFT spectra illustrated in Figure 16.

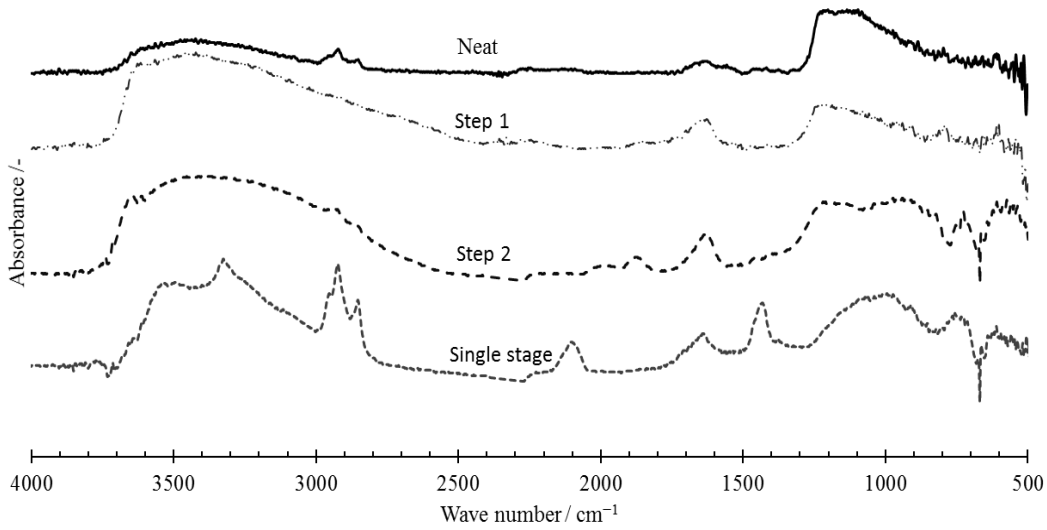

Figure 16. DRIFT spectra of silicon during the various processing stages.

As illustrated in Figure 16 there is a clear shift in band intensity for each sample. The oxide band intensity increased during the first stage as indicated by the larger band around 1100 cm^{-1}. The intensity of this band decreased after the silicon was exposed to hydrofluoric acid. Hydrogen passivation of the surface was confirmed by the presence of bands at 2100 cm^{-1} and 2250 cm^{-1}. These results confirmed that both processes altered the silicon surface chemistry

and structure. The effect these changes could have on combustion performance needs to be investigated.

5.3 Magnesium hydroxide

Magnesium hydroxide was used initially as a filler to test the safety of compounding and extrusion operations. It was used as received in all stages of the process. XRF and XRD analysis of the powder is shown in Table 15 and Figure 17.

Table 15. XRF analysis of magnesium hydroxide.

Element	Mg	Fe	Si	Ca	Ba	I
wt.%	98.82	0.01	0.12	0.32	0.32	0.15

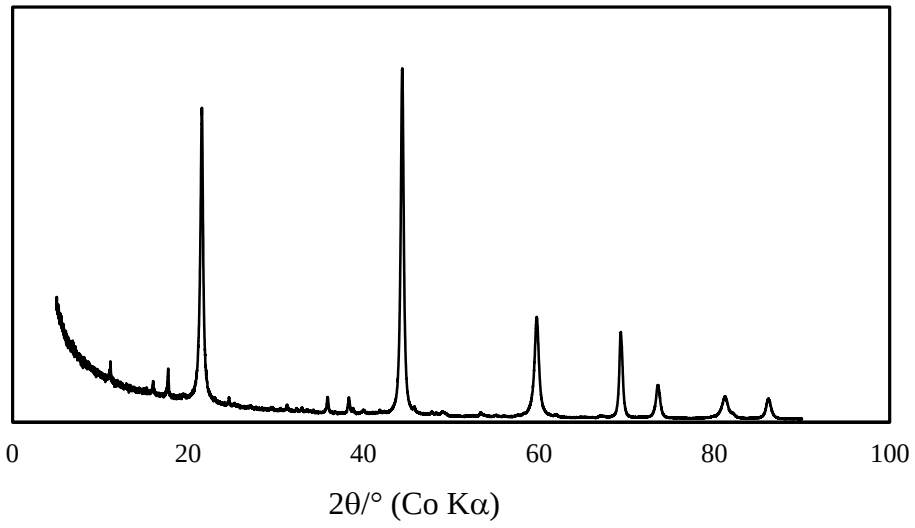

Figure 17. XRD results of magnesium hydroxide.

The particle size distribution of the sample was also determined as displayed in Table 16 and Figure 18.

Table 16. Particle size distribution of the magnesium hydroxide.

D_{10}(µm)	D_{50}(µm)	D_{90}(µm)
2.4	20.2	47.7

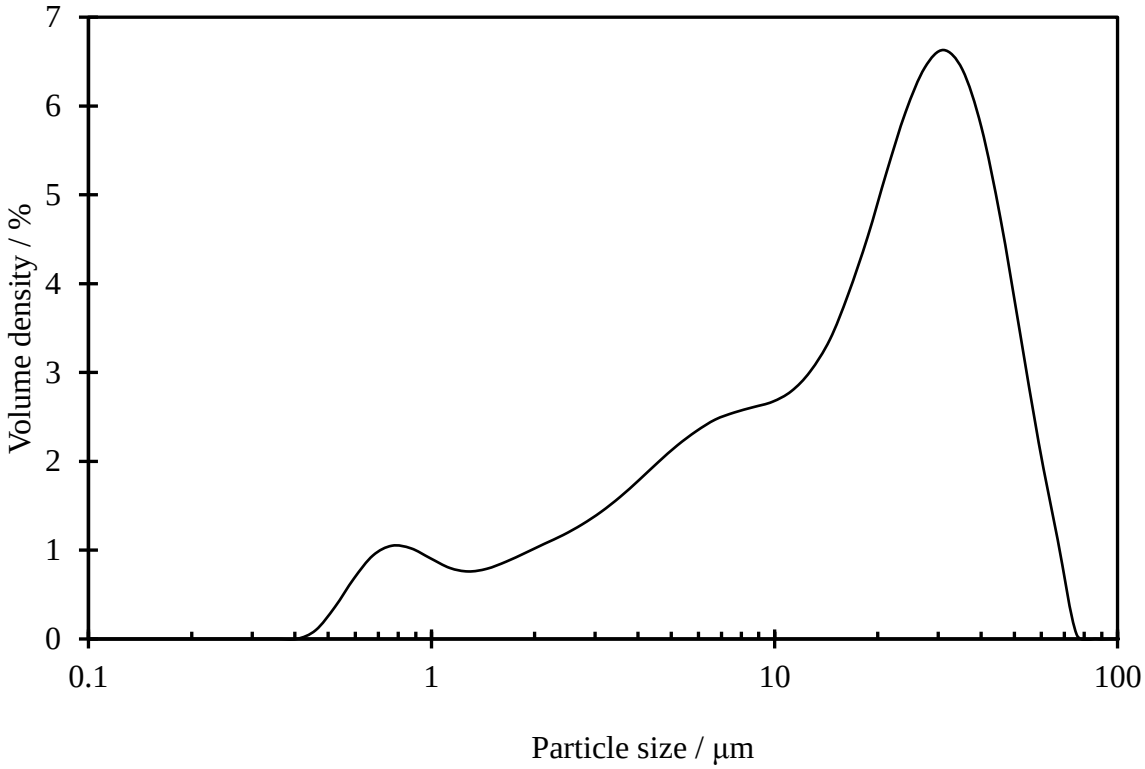

Figure 18. Particle size distribution of the magnesium hydroxide.

The double peaked nature of the distribution illustrated in Figure 18 indicates that there is agglomeration present. The magnesium hydroxide used also demonstrates a wider distribution range than the aluminium used. This was expected since it was not sieved before use.

5.4 Polymer characterisation.

5.4.2 Thermal analysis

TGA analysis was performed on all of the polymers used. The results of the analysis are shown in Figure 19 to Figure 21.

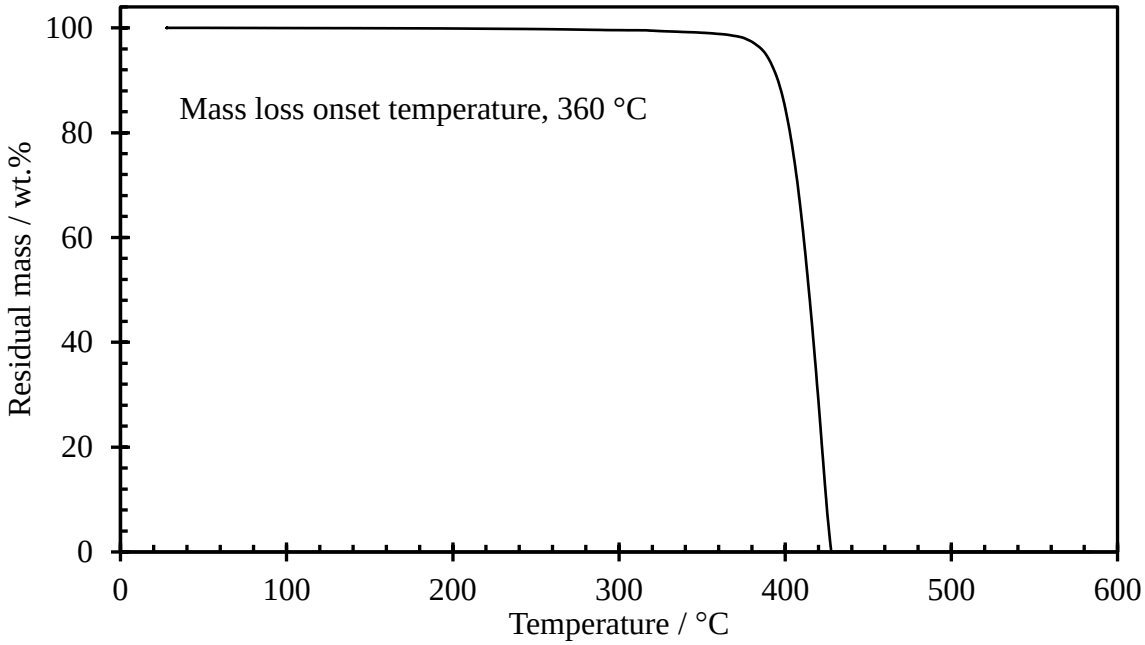

Figure 19. TGA curve for FK-800®.

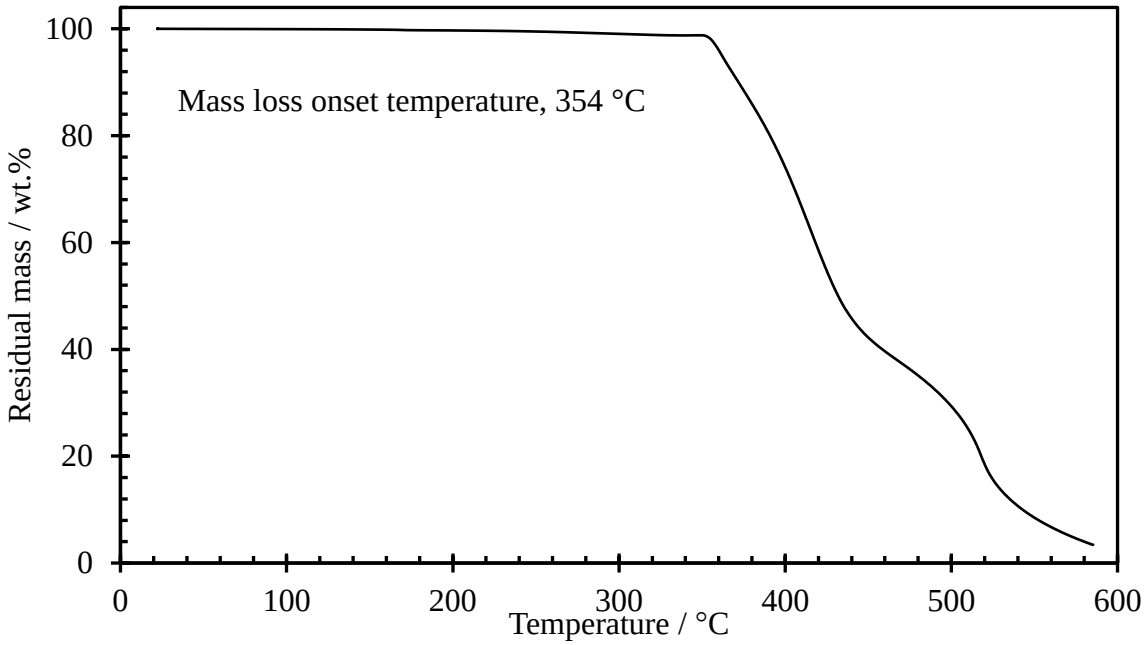

Figure 20. TGA curve for Dyneon 31508®.

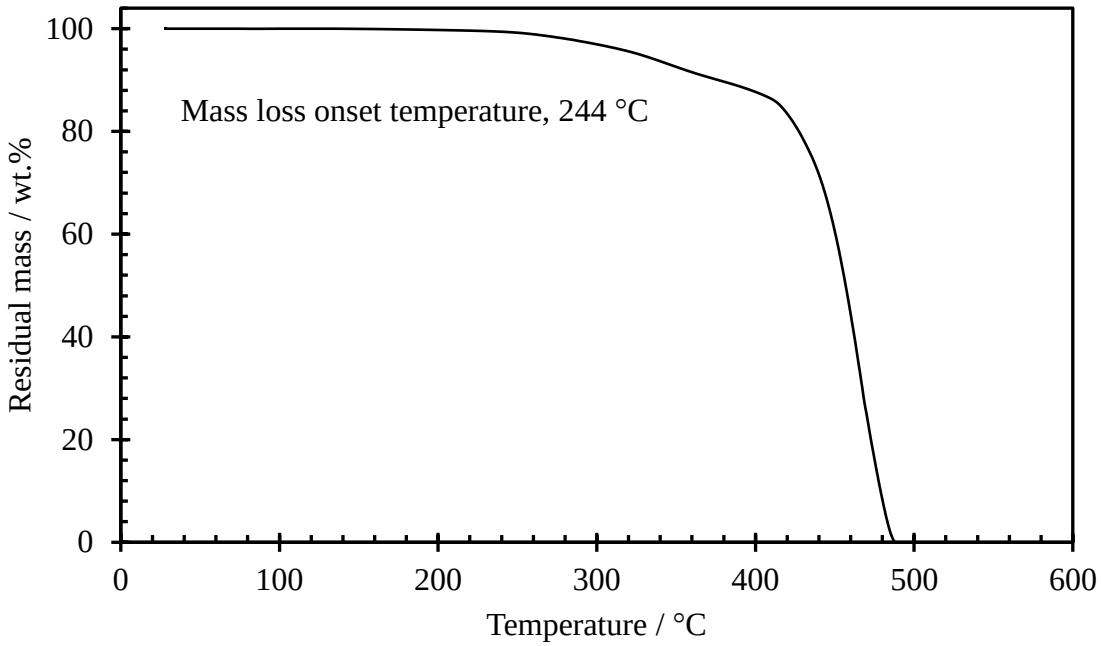

Figure 21. TGA curve for LFC-1®.

From the results depicted in the preceding figures it is clear that mass loss is initiated at much higher temperatures for FK-800® and Dyneon 31508®. With LFC-1® starting to lose mass at a considerably lower temperature. The addition of LFC-1® to the systems will therefore limit the processing temperatures of the compositions. How this affects the ignition temperature of the composition should be studied before extrusion or printing can be attempted. For this purpose DTA analysis was employed as discussed later on.

5.4.1 Rheology

Rheological studies were performed on the selected polymers as well as a polylactic acid (PLA). This was done for comparative purposes due to PLA's widespread use for FDM. The results of the rheological tests are illustrated in Figure 22.

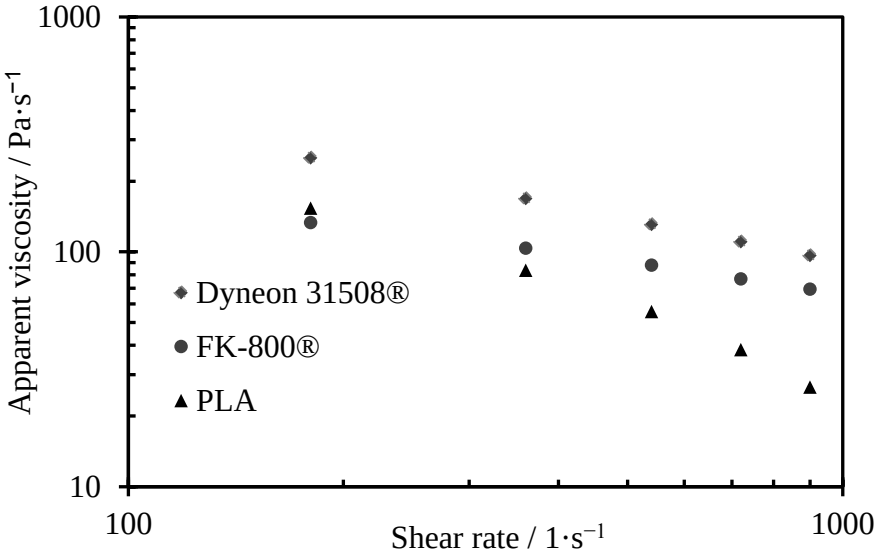

Figure 22. Apparent viscosity as a function of shear rate for the oxidisers.

From Figure 22 it was clear that PLA had the lowest apparent viscosity over most of the range of shear rates illustrated. At lower shear rates however unfilled FK-800® had the lowest viscosity. This was not the case with filler added to the polymer. The addition of the inert filler caused a drastic upwards shift in the apparent viscosity of the FK-800® system. This is illustrated in Figure 23.

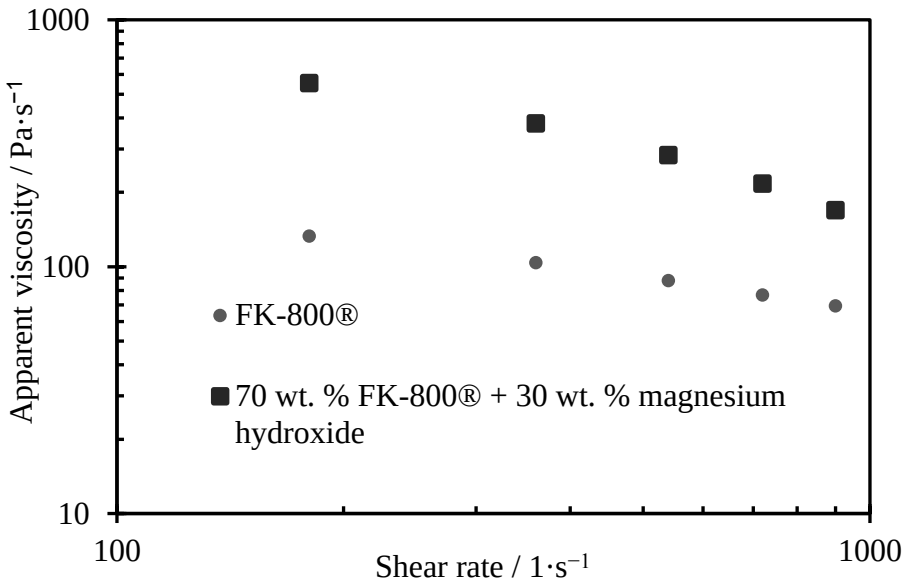

Figure 23. Effect of filler on the apparent viscosity of FK-800®.

The drastic increase in viscosity at low shear rates may prove problematic when attempting to process the polymer. This is especially true when it comes to 3D printing the polymer. As FDM type extruders force the melt through the printer nozzle by continuously feeding a polymer filament to the hot end. This action does not allow for high pressure generation. Which in turn means that printing viscous melts may prove problematic as constant flow may not be achievable. This led to the addition of LFC-1® with the intention of reducing the melt viscosity of the polymers.

6. Simulation results

Simulations for the reactions of aluminium and silicon with the fluoropolymers were done under conditions that replicated the conditions in the bomb calorimeter. Figure 24 and Figure 25 compares the maximum adiabatic temperature as well as the enthalpy change per gram composition for the systems.

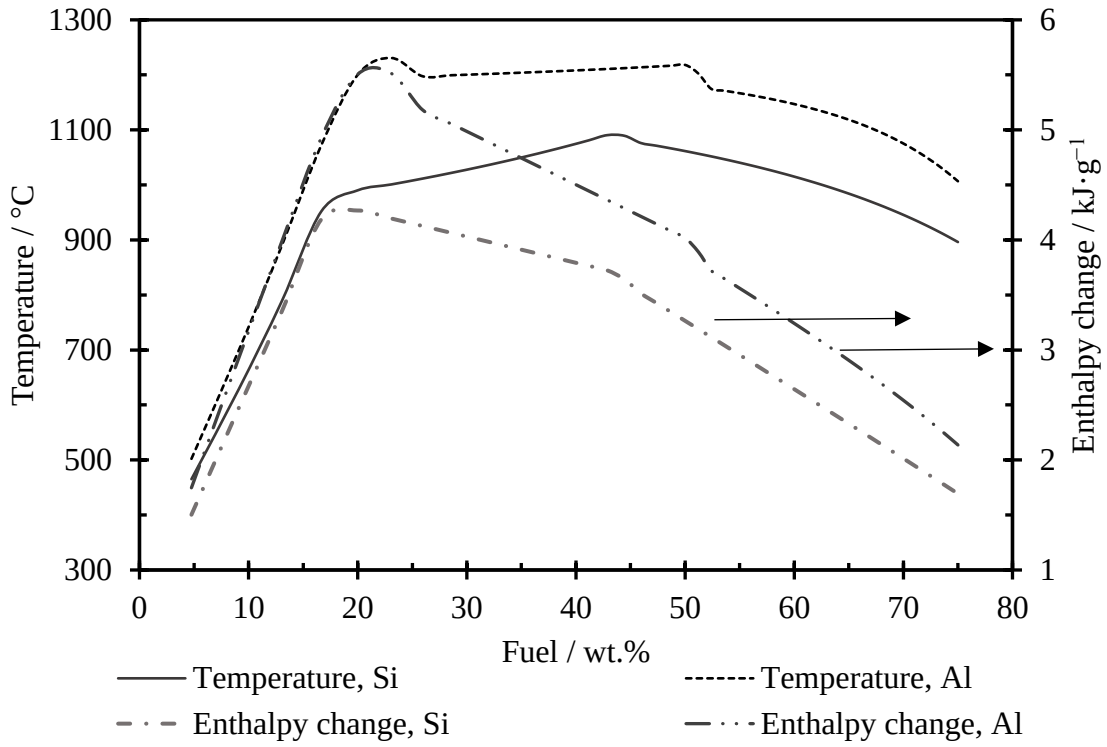

Figure 24. Temperature and enthalpy release for FK-800® containing systems.

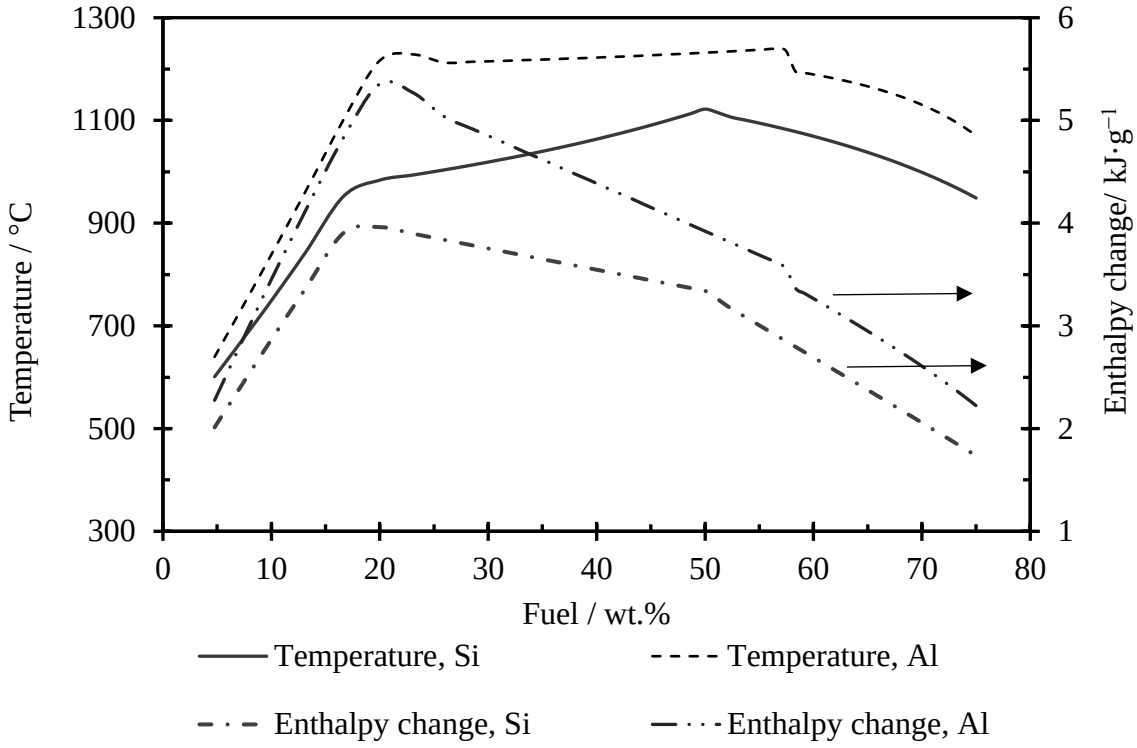

Figure 25. Temperature and enthalpy change for Dyneon 31508® containing systems.

It was clear from the simulations that aluminium was the more energetic fuel between the two. This was indicated by the higher enthalpy changes as well as higher adiabatic temperatures achieved. For both oxidisers silicon requires a higher fuel loading than the aluminium to reach its maximum temperature. Which could lead to processing problems due to a much higher solids loading. The oxidisers had little difference between them when comparing the temperatures and energies obtainable for the two fuels. The change in the state of products per gram composition as well as the overall conversion for the fuel in each system is shown in Figure 26 and Figure 27.

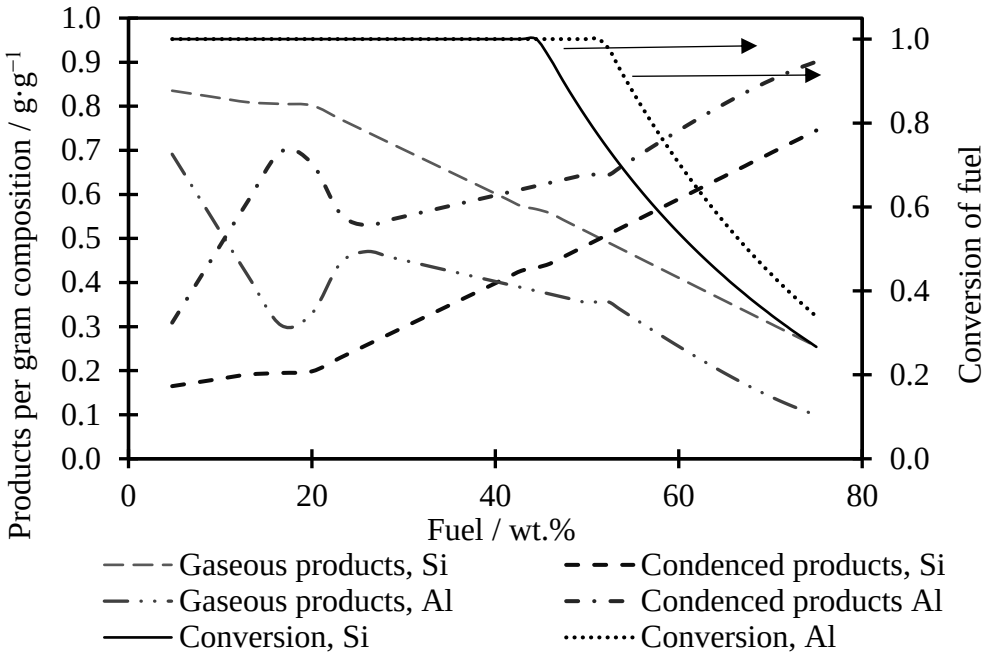

Figure 26. Products produced per gram composition consumed with conversion of fuel using FK-800® as an oxidiser.

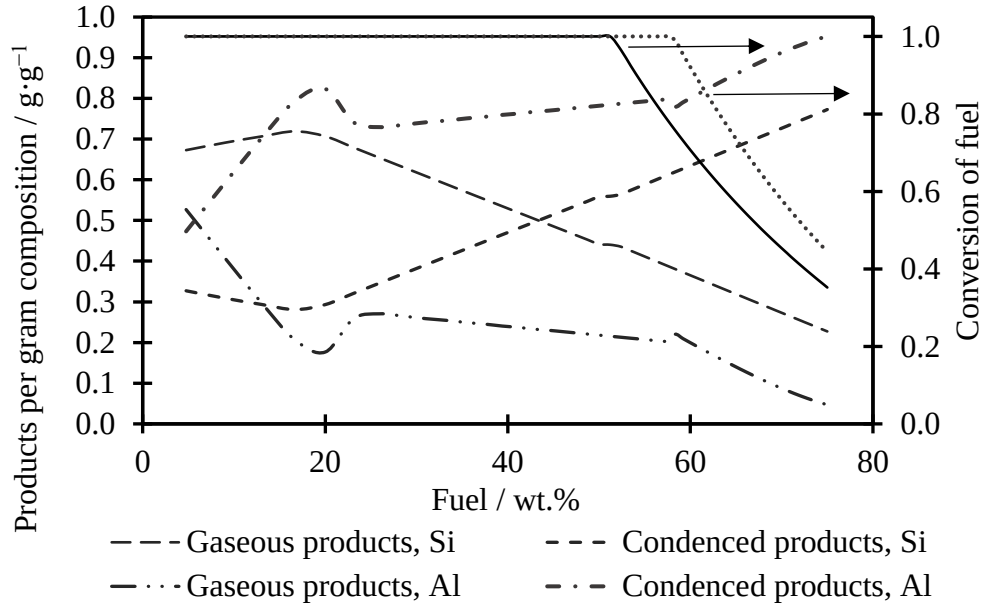

Figure 27. Products produced per gram composition consumed with conversion of fuel using Dyneon 31508® as an oxidiser.

For all systems the simulations indicate that increased fuel loads lead to increases in condensed products formed. By altering the fuel ratio the system can potentially be tailored in order to suit multiple end applications. For example low gas production will be better suited for pyrotechnic time delays. Which is easily obtainable under the conditions simulated for aluminium. For silicon however a fuel loading of greater than 52 wt.% and 43 wt.% is required in order to minimise the gas output. It should be noted that under bomb calorimeter conditions the pressure is much higher than what is experienced under an open burn. This means that the amount of gas produced may be significantly less than what will be experienced in an open air simulation or burn. There is a limit however as to how much fuel can be added depending on the polymer incomplete combustion starts to be a factor above 45 wt.% and 50 wt.% for FK-800® and Dyneon 31508®. In an open air burn this may not be a problem as oxygen from the surroundings can contribute to the reaction.

Another factor to consider would be the products of combustion. These systems have the potential to release hydrofluoric acid, chlorine, hydrochloric acid (HCl), silicon tetrafluoride (SiF_4), and other compounds during combustion which can be a health hazard. These hazards include chemical burns, respiratory tract irritation and even death. This will be especially problematic if used in confined spaces. Reducing production of these should therefore be considered when the application of the system is being considered. Release of hydrofluoric and hydrochloric acids are possible due to the fact that the polymers used are not perfluorinated. While silicon tetrafluoride is the main combustion product of the silicon systems. Figure 28 and Figure 29 show some of these products of combustion as a function of fuel load.

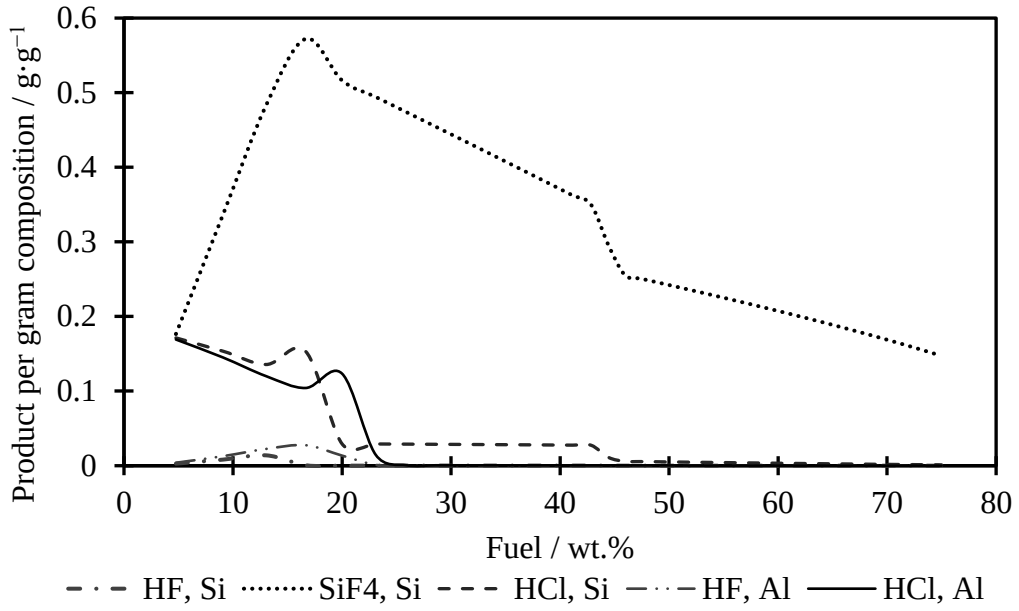

Figure 28. Effect of fuel load on the production of certain components with FK-800® as an oxidiser.

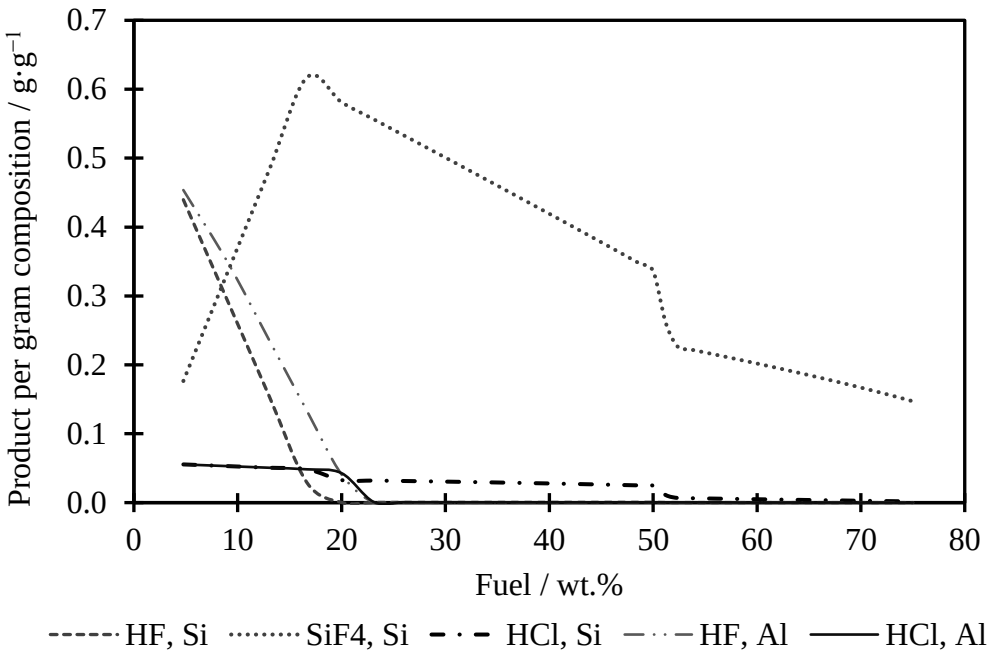

Figure 29. Effect of fuel load on the production of certain components with Dyneon 31508® as an oxidiser.

For both polymers the release of hydrofluoric acid and hydrochloric acid is only possible at low fuel loads. Dyneon 31508® however has a much higher initial release of hydrofluoric acid while FK-800® has a much higher hydrochloric acid release. This makes sense when looking at the constituent components of each copolymer. The compositions are almost exactly the inverse of one and other. This means that FK-800® which consists of 83.74 % CTFE has a significantly higher chlorine content. While the 81.4 % VDF content of Dyneon 31508® may offer an explanation for the increased presence of hydrofluoric acid due to the greater amount of hydrogen and lower chlorine content of the system.

Using silicon as a fuel leads to a significant release of silicon tetrafluoride. At a fuel load of 17 wt.% around 60 wt.% of the original mass gets converted to silicon tetrafluoride. This allows for the maximum release of energy as shown in Figure 24 and Figure 25. If the release of this compound should be limited due to operational requirements higher fuel loads are necessary. Increasing the silicon content above 45 wt.% and 50 wt.% for FK-800® and Dyneon 31508® systems leads to a significant drop in the release of silicon tetrafluoride. This however leads to reduced energy output due to incomplete combustion.

From these simulations it was clear that aluminium provides better energetic performance than silicon. Silicon also had the added risk of producing higher levels of toxic combustion products. The fact that this was the main combustion product lead to its exclusion from further studies. Aluminium systems had optimal fuel loadings of 23 wt.% and 20 wt% for the FK-800® and Dyneon 31508® oxidisers.

7. Experimental results and discussion

7.1 DTA

DTA analysis was done in order to determine at which temperature ignition takes place as well as which phase change is the likely cause of ignition. These points were identified by means of tangent analysis on the endotherms and exotherms. This was done in order to obtain a better understanding of the nature of the reaction between the polymers and the fuels. All of the compositions contained a fuel load of 30 wt.%. The results are illustrated in Figure 30 to Figure 34.

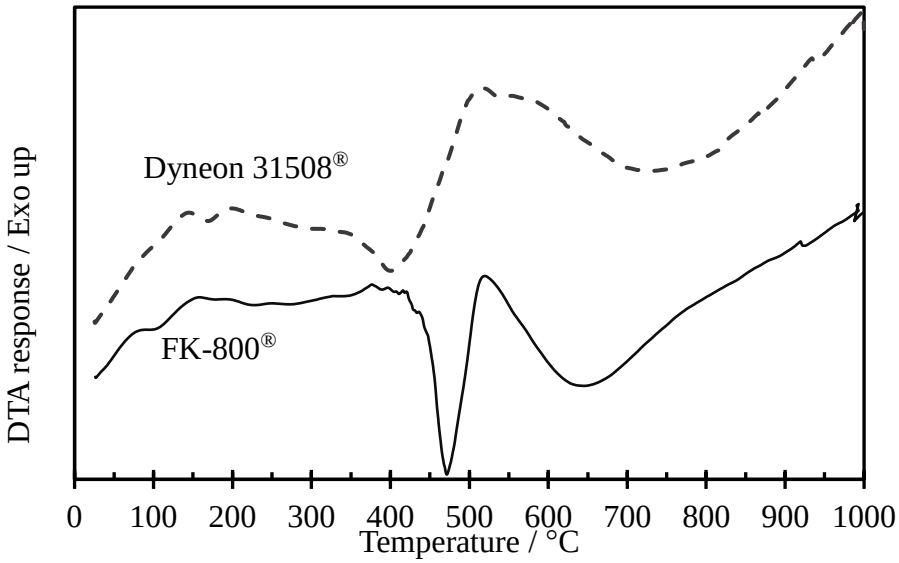

Figure 30. DTA response for the selected oxidisers with the addition of 10 wt. % LFC-1®.

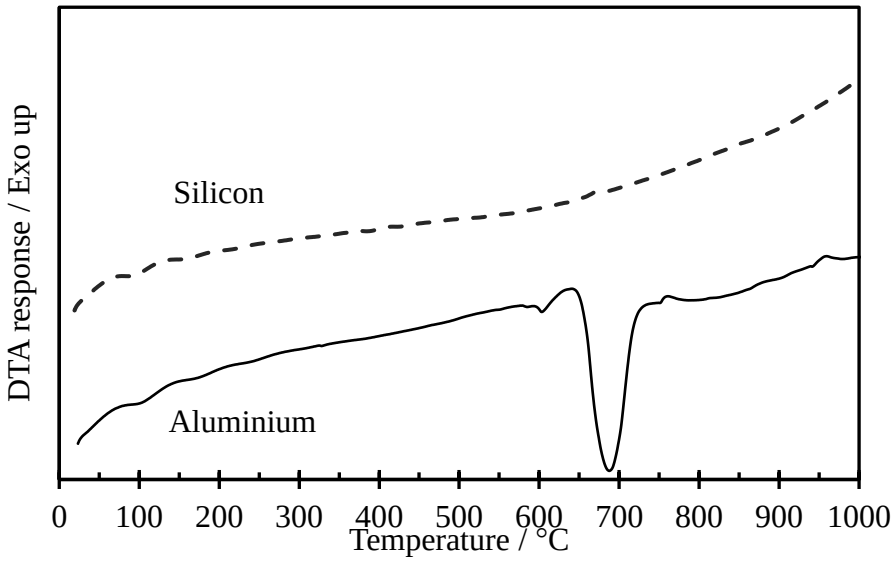

Figure 31. DTA responses for the fuels investigated.

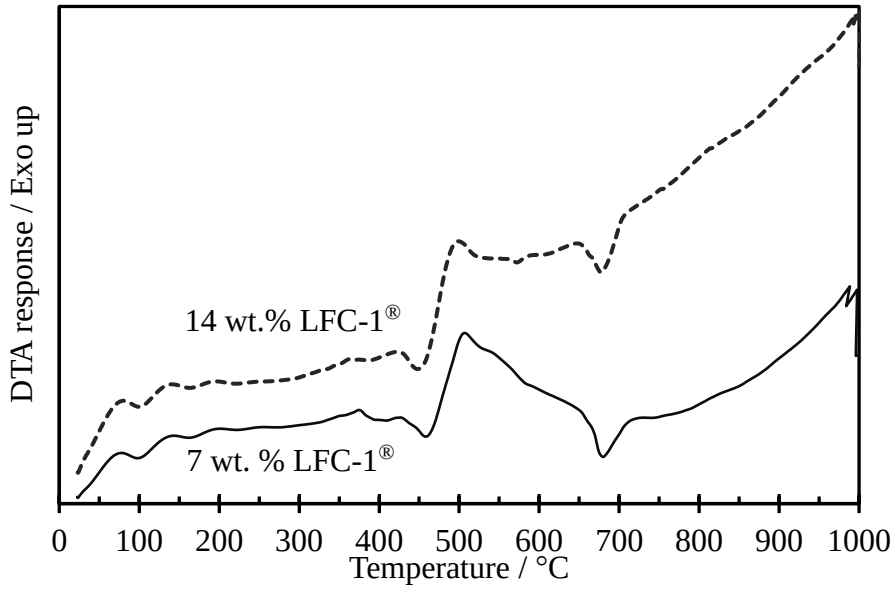

Figure 32. DTA responses for aluminium and FK-800® systems with different LFC-1® loadings.

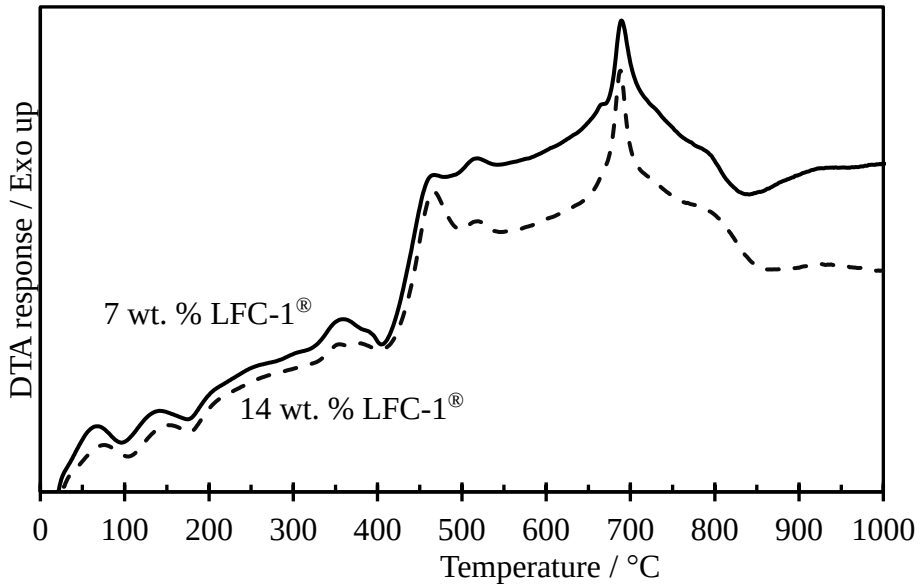

Figure 33. DTA responses for aluminium and Dyneon 31508® systems with different LFC-1® loadings.

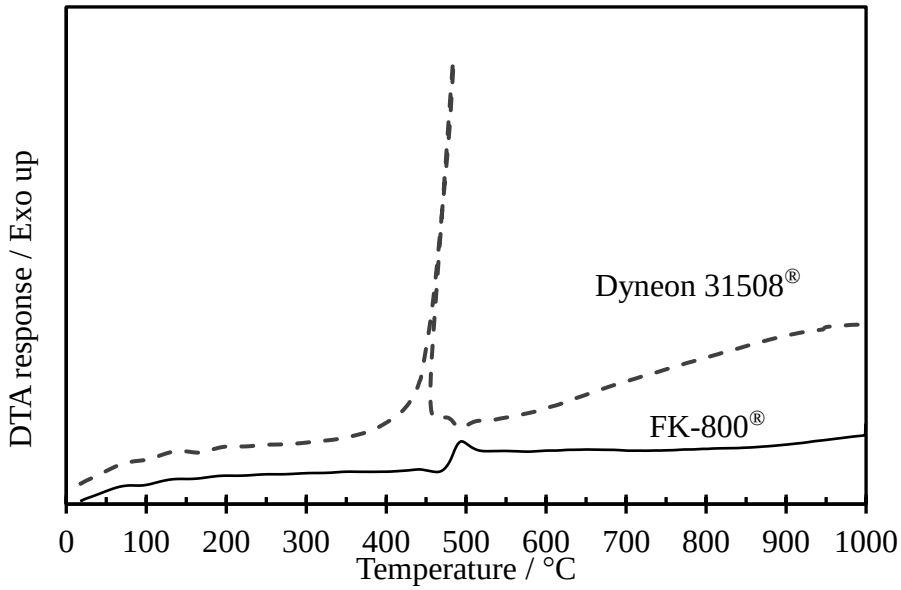

Figure 34. DTA responses for silicon systems with the oxidisers and 7 wt.% LFC-1®.

Both oxidisers are known to degrade above 350°C as confirmed by TGA analysis. Figure 30 confirms that Dyneon 31508® degradation starts at a lower temperature than FK-800® when both of the samples contain a similar loading of LFC-1®. The change in the state of the oxidisers happens at much lower temperatures than that of the fuels. This is evident when comparing the placement of the endotherms in Figure 30 and Figure 31. As expected, silicon did not show any indication of undergoing a phase change. While aluminium has a melting endotherm at a

much higher temperature than those of the polymers. This endotherm was still visible in Figure 32. This implies that the reaction taking place is a solid-gas reaction between the fuel and the decomposition products of the polymers. Indicating the systems' ignition temperature is influenced to a greater degree by the degradation of the oxidiser than phase changes occurring in the fuel. This is due to the relatively high temperatures at which these changes occur in the fuels. The presence of this endotherm may be indicative of unreacted aluminium present in the system. Using Dyneon 31508® as the oxidiser a second exotherm visible in place of the expected melt endotherm for aluminium. The occurrence of which is illustrated in Figure 33. The reason for this is not yet known as a change to silicon fuel did not result in a similarly shaped graph. Changing the fuel to silicon however showed little to no difference in the ignition temperatures of the FK-800® systems as is shown in Figure 34. With the ignition temperatures being approximately that of the aluminium systems with similar LFC-1® loads. This further strengthens the argument for a solid-gas reaction controlled by oxidiser degradation for the FK-800® system as both fuels showed similar ignition temperatures.

Increasing the LFC-1® content of the composition from 7 wt. % to 14 wt. % for the aluminium causes a shift the ignition temperatures as shown in Figure 32 and Figure 33. For the FK-800® the ignition temperature drops from approximately 460 °C to approximately 450 °C while for the systems containing Dyneon 31508® the temperature decreases from approximately 380 °C to 365 °C. This was thought to be due to the drastically lower degradation temperature of LFC-1®.

7.2 Extrusion

The aluminium containing systems were extruded at a fuel rich loading of 30 wt.%. This loading was chosen due it being having the highest enthalpy of combustion as shown by bomb calorimetry (Cowgill, 2017). In order to reduce the melt viscosity LFC-1® was added during compounding. This addition was done by replacing 10 wt.% or 20 wt.% of the polymer mass with LFC-1® equating to 7 wt.% or 14 wt.% of the total composition. Reducing the melt viscosity was required as the rheological tests indicated earlier and was further supported by preliminary extrusion trials using the inert filler done by Cowgill (2017).

This viscosity reduction would be important when the composition has to be 3D printed as the pressure gradient in the printer head is relatively small. The thermal analysis of the polymers discussed in previous sections had indicated that processing should take place below 240°C.

The initial wax loading attempted was 7 wt.%. The extrusion parameters are listed in Table 17 with the result of the filament extrusion illustrated in Figure 35. The initial extrusion using the same parameters as those used for the magnesium hydroxide filled polymer led to some defects. The roughness of the extruded filament is clearly visible in Figure 35. This defect indicated that the melt viscosity was still too high at the temperature profile to allow for a smoother more uniform strand to be extruded.

Table 17. Extrusion parameters.

Parameter	Value
Screw speed (RPM)	2280
Zone 1 temperature (°C)	210
Zone 2 temperature (°C)	220
Die temperature (°C)	230

Figure 35. Section of extruded FK-800® filament.

Increasing the wax content to 14 wt.% was the next stage for the FK-800® aluminium system. The higher wax loading proved to sufficiently reduce the viscosity of the melt for improved extrusion results. This allowed for more controlled filament diameters to be achieved as well

as a smoother extrusion profile to be obtained. Both of which is beneficial when trying to feed the filament to a 3D printer.

Mixing was however not sufficient with this approach. The result was made apparent during testing as discussed in the following section. A different compounding method was attempted in order to improve the mixing quality of the system. This method utilised a twin screw extruder in a co-rotating configuration. Four compositions were extruded on this extruder. The aluminium loading was maintained at 30 wt.% for all of the compositions. Oxidisers were changed between FK-800® and Dyneon 31508®. LFC-1® was added to all systems as either 7 wt.% or 14 wt.%. The extrusion parameters for both systems are summarised in Table 18. A much smoother profile was obtained for the systems. This indicated an improvement in the compounding and extruding quality.

Table 18. Twin-screw extrusion parameters.

Parameter	Value
Zone 2 temperature (°C)	140
Zone 3 temperature (°C)	170
Zone 4 temperature (°C)	180
Zone 5 temperature (°C)	190
Zone 6 temperature (°C)	200
Zone 7 temperature (°C)	210
Zone 8 temperature (°C)	220
Die temperature (°C)	230
Screw speed for FK-800® systems (RPM)	320
Screw speed for Dyneon 31508® systems (RPM)	305

7.3 Energetic properties of extruded filaments

7.3.1 Burn rates

Burn rate measurements were the initial gauge of mixing quality. This method has found widespread use as a metric for combustion performance(Fleck et al., 2017). Initial burn tests were conducted on the two FK-800® compositions extruded on the single screw extruder. These two systems differed by having an LFC-1® loading of either 7 wt.% or 14 wt.%. Obtaining burn rate measurements were problematic as the flame front could not be maintained consistently. When burn rates could be measured significant variance was witnessed. The variance was approximately 40 % of the mean value for both compositions. The reason for this was thought to be due to incomplete mixing that occurred during the compounding stage. This was supported by the density calculations done on all samples burnt. The densities of the two composition types had a variance ranging between 16 % and 19 %. This variation in sample density can contribute significantly to variations witnessed in pyrotechnic burn rates. It was indicative of unequal distribution of constituent components throughout the composition.

Burn tests were conducted on films cast from the solution to further test this theory. The films burnt in this manner showed similar deviations as the filaments. Which may prove that solvent based compounding provides insufficient mixing for accurate burn rate characterisation. The FK-800® samples were studied under a microscope to support the theory. The results of which are illustrated in Figure 36.

A difference could be seen in the aluminium distribution across the thickness of the films as well as the surfaces. The aluminium density increased towards the bottom part of the film as illustrated in Figure 36 a-b and e-f. This indicates that settling occurred during the time it took the solvent to evaporate from the cast films. Viewing cross sections of the extruded filaments revealed unequal aluminium distribution along the length of the filaments. The analysis also showed several regions in which pores or cavities had developed. These two factors explains the variance in density. Which led to the variance in burn rates witnessed.

After switching compounding methods, analysis of the samples were repeated. As with the initial samples, compositions still had problems with maintaining the flame front. This was theorised to be due to the fact that the majority of the generated heat was escaping before it could effectively ignite the next layer of the composition. The simulations had shown that a significant portion of the combustion products would be gaseous. With these products freely leaving the system heat was being dissipated into the surrounding at a rate greater than what could maintain stable progression of the flame front. Furthermore minimal amounts of these gaseous products could penetrate the unreacted composition when compared to other particulate compositions. This would be due to the low porosity of the extruded filament. Penetration of subsequent unreacted layers of the composition by heated reaction products assists in transmitting the flame front by pre-heating the unreacted material.

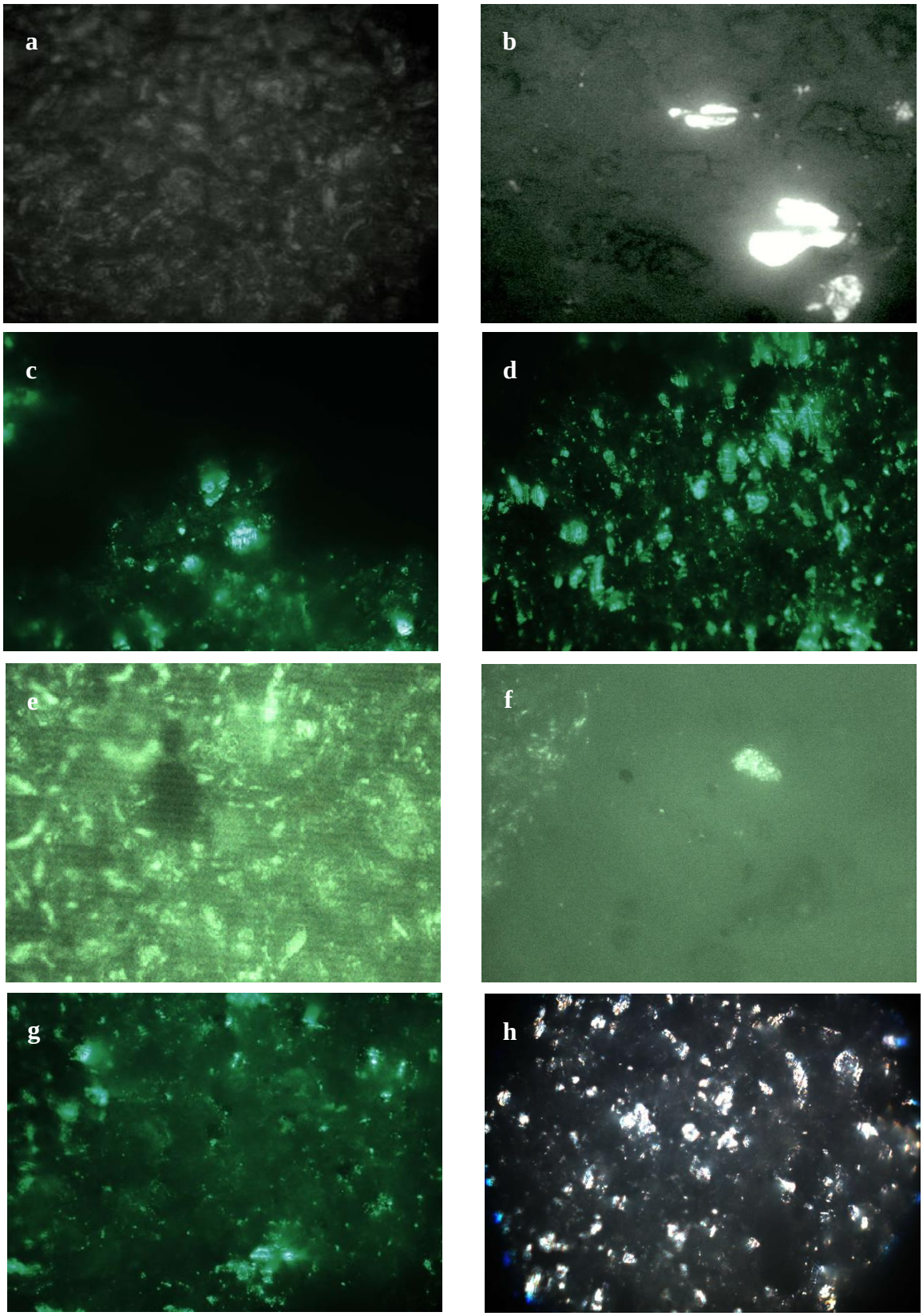

Figure 36. Film with 7% LFC-1® (a) top and (b) bottom. (c-d) Filament 7 with % LFC-1®. Film with 14 % LFC-1® top (e) and bottom (f). Filament with 14 % LFC-1® (g-h).

In order to address the problem mentioned a shift was made to a partially enclosed system. This was done by placing an alumina tile over the sample holder. The alterations made to the system drastically improved the combustion performance for two of the four systems, as summarised in Table 19.

Table 19. Results of burn tests.

Oxidiser	LFC-1® (wt.%)	Maximum burn temperature (°C)	Burn rate ($mm \cdot s^{-1}$)	Variance (%)
FK-800®	7	794	15.9	14
FK-800®	14	971	18.9	25
Dyneon 31508®	7	1004	-	-
Dyneon 31508®	14	1020	-	-

By partially enclosing the system there was a drastic improvement in the reproducibility of the burn tests for the FK-800® systems. It could however not assist with the reproducibility of Dyneon 31508® system burns. Neither of the Dyneon 31508® systems have burn rates listed in Table 19. These systems would ignite and burn violently for a section before extinguishing themselves. The systems burnt with an audible crack and bright flash. The lengths of the sections that were consumed during these reactions were however too unpredictable to make any useful measurements. Burn temperatures could however be obtained for these two systems. Burn temperature was clearly influenced by the LFC-1® content of the system. For both oxidisers an increase in burn temperature was witnessed as the LFC-1® loading was increased.

The same trend is illustrated in Table 19 for the FK-800® systems when comparing the burn rates. There are two possible explanations for the increased burn rates obtained at the higher LFC-1® loads. The lower decomposition temperature of LFC-1® sensitises the system leading to a lower ignition temperature by providing fluorinated decomposition products at lower temperatures than FK-800®. Along with this there was also an increase in the reaction temperature. An increase in reaction temperature increases the rate at which it occurs.

7.3.2 Time to ignition

To further characterise the energetic differences between the compositions laser ignition studies were performed. Time to ignition's dependence on the power of the laser beam is illustrated in Figure 37 and Figure 38.

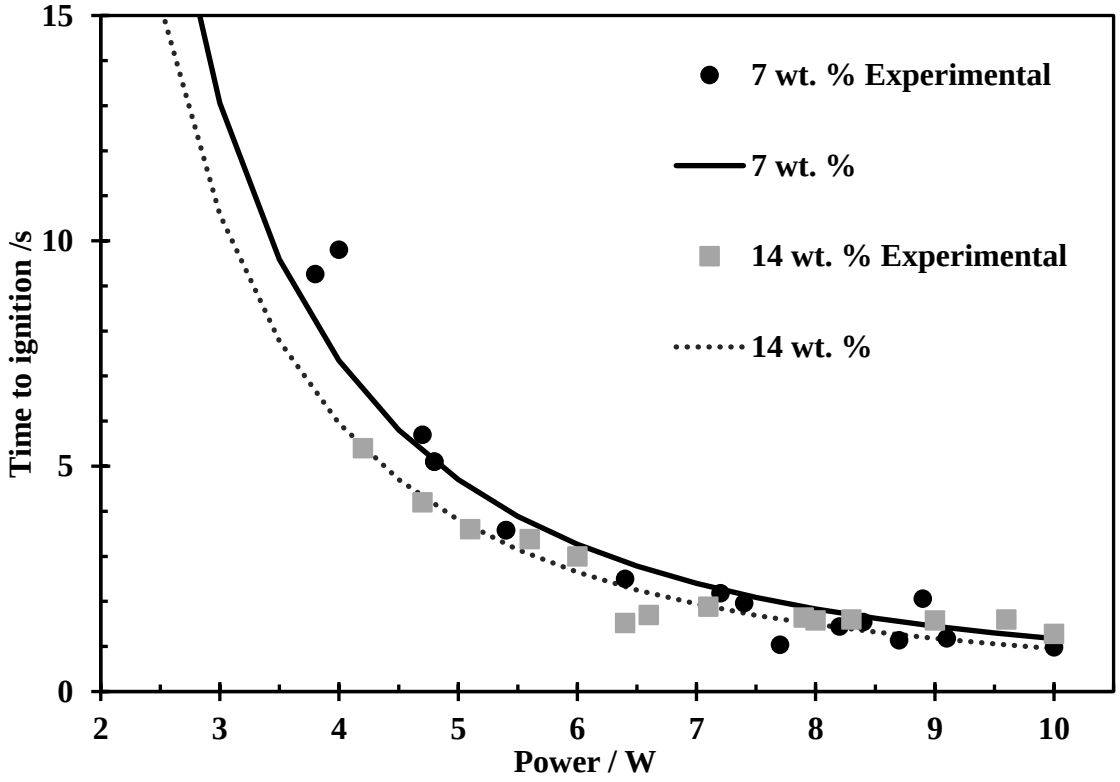

Figure 37. Ignition tests for aluminium FK-800® with the two LFC-1® loadings.

An increase in LFC-1® loading decreased the time to ignition for the FK-800® system while the opposite was true for the Dyneon 31508® system. The FK-800® systems seem to have a shorter delay time than those of the Dyneon 31508® systems. In an attempt to quantify the effect of the LFC-1® addition as well as compare the two main oxidisers, trend lines were plotted in the figures. The trend lines for the time to ignition (t_{ign}) curves shown are described by equation 8 (Fang and Ahmad, 2016).

$$t_{ign} = \frac{\pi}{4\alpha}\left[k\left(T_{ign} - T_0\right)\right]^2 \frac{1}{q^2} \tag{8}$$

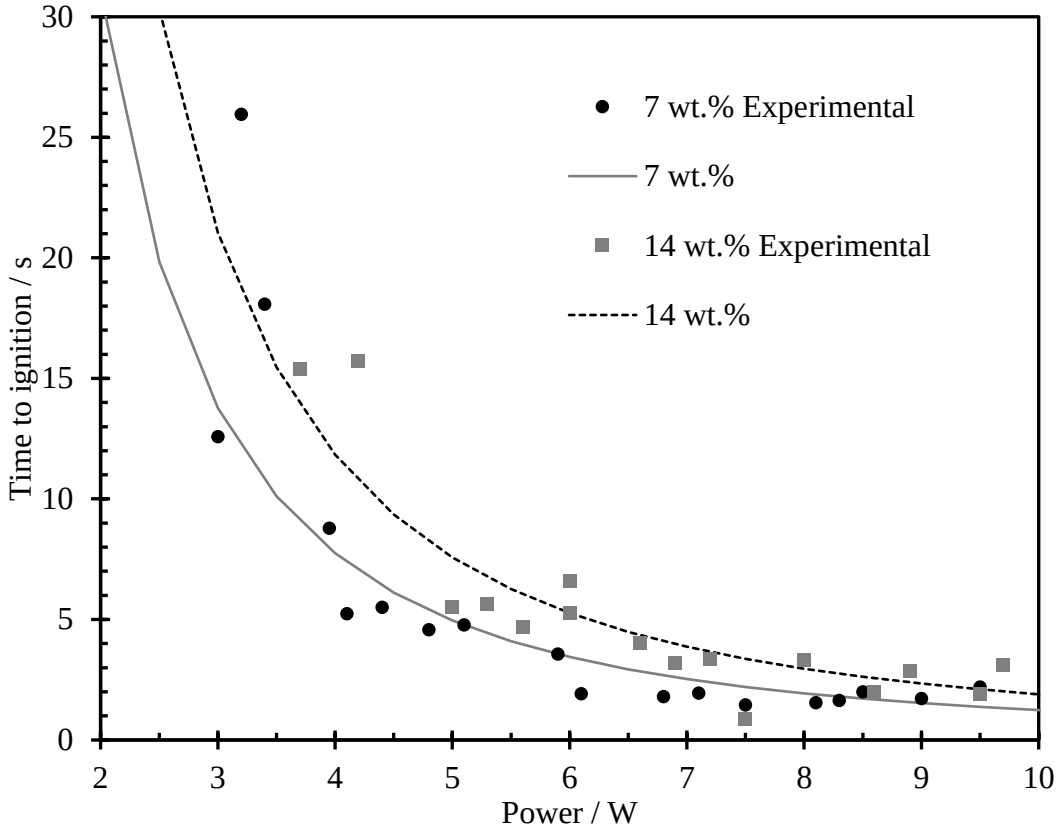

Figure 38. Ignition tests for aluminium Dyneon 31508® with the two LFC-1® loadings.

From this equation it is clear that the ignition time is dependent on both the laser and thermal properties of the composition. The ignition temperature (T_{ign}) of the samples was determined from DTA analysis performed while the starting temperature (T_0) was taken as the ambient conditions. Thermal diffusivity (α) is related to thermal conductivity (k) as illustrated by equation 9.

$$\alpha = \frac{k}{\rho C_p} \tag{9}$$

Heat flux (q) was calculated from equation (10).

$$q = \frac{P}{A} \tag{10}$$

The variables in equation 15 are the power (P) and area (A) of the laser. Equations 9 and 10 were substituted into equation 8 to get equation 11 with some rearrangement of unknowns into a variable as shown in equation 12.

$$t_{ign} = \frac{\pi}{4} B\left[\left(T_{ign} - T_0\right)\right]^2 \frac{A^2}{P^2} \tag{11}$$

$$B = \frac{k^2}{\alpha} \tag{12}$$

The value of *B* was altered in order to obtain the best fit for the graphs. The values obtained in this manner are listed in Table 20. The results in Table 20 are only to probe the effect of the compositional changes on the time to ignition. This represents an oversimplification of the true situation. Multiple complex heat transfer, chemical and physical processes are occurring up to the point of ignition. Furthermore, the assumption would have to be made that the sample acts as an inert material up until the point of ignition for these equations to be of any use. However, for the purposes of comparing the four systems it was deemed to be sufficient.

Table 20. Values of B for the compositions tested.

Composition	**B** $(kJ^2 \cdot s^{-1}\ m^{-4}\ K^{-2})$
FK-800® 7 % LFC-1®	146. 5
FK-800® 14 % LFC-1®	123
Dyneon 31508® 7 % LFC-1®	185.4
Dyneon 31508®. 14 % LFC-1®	283.4

Values calculated for the variable *B* clearly showed that the system with the shortest ignition delay time was the FK-800® system with a 14 wt.% LFC-1® load. Both of the Dyneon 31508® systems had longer delay times. The combination of two polymers with comparatively lower degradation temperatures may be contributing to the removal of energy from the system as they undergo endothermic phase changes and degradation. These processes occur at a temperature too low for ignition to take place. Ignition is therefore delayed as the remaining material experiences a slower temperature increase due to increased heat loss. This is supported in part by the DTA results. It was shown that a second exotherm formed at the temperature that one would expect to witness an endotherm associated with the melting of aluminium. This may suggest that in this case ignition is initiated by a phase change in aluminium. Another factor

that was potentially contributing to the trend witnessed, was interference by degradation products. Before ignition occurred a visible smoke or vapour cloud was being released from the sample. The material in this phenomenon could affect the amount of energy reaching the sample as the laser light gets scattered or absorbed by the matter contained within region between the lens and the sample.

As shown by the DTA results for FK-800® the addition of LFC-1® lowers the ignition temperature. This is probably due to it providing some fluorinated decomposition products in a temperature range that would allow for aluminium to start reacting with it before the bulk of the FK-800® could decompose. Thereby decreasing the ignition delay. This also contributes to the increased burn rates witnessed.

7.4 Printing results

Preliminary printing proved problematic. The initial printer setup could not handle the viscosity of the polymer melts. Which led to regular blockages which in turn led to degradation of the polymer within the printer hot end. The addition of LFC-1® did not decrease the melt viscosity to the extent that the melt would flow with ease. It did however lead to another problem occurring which was an overly flexible filament. The flexible filament could not provide sufficient pressure to allow for the polymer melt to be extruded through the nozzle as it would wind around the feeder gear when the melt started to resist flow.

Increasing the printing temperature above 230°C could not be considered for a number of reasons. The first being how close the printing temperature was to the temperature at which mass loss is initiated within LFC-1®. Heat flow up the filament was another problem that had to be overcome. Initial prints using magnesium hydroxide as a filler material did not have a problem of premature swelling or softening of the strand, but it caused severe feeding issues for the aluminium filled systems. As the strand was being fed into the hot end it would start swelling within the feeding tube due to heat traveling up the side walls and the filament itself. This caused swelling and softening of the filament at a distance from the heating block leading to blockage.

Several alterations were needed in order to successfully print with the compositions in question. A change to a larger diameter nozzle was made in order to reduce the pressure required to force the melt out of the extruder. The nozzle diameter had to be increased to a diameter of 1.2 mm from the original 0.4 mm before flow could be achieved. Due to excessive swelling in the feeder tube it was enlarged to 2.4 mm. Even with these changes the feeding was still problematic as the resistance to flow would quickly build up once printing started. Which led to the feeding gear being entangled by the flexible filaments.

In order to achieve prints with the compositions as is without further compositional changes staged printing had to be employed in an attempt to avoid significant feed problems. This meant that a short strand of composition was forced through the printer using a more rigid filament consisting of PLA taking care not to deposit any PLA onto the part being printed. Once a layer had been lain down the print was paused allowing the feeder tube to cool down with no material within it. This meant that progress was slow and printing quality was not of a high standard. An example of a print is displayed in Figure 39.

Figure 39. Example of an FK-800® print.

Layer control proved to be problematic whether feeding by gear or by hand since the system was prone to blockages. This led to the bulging sections in Figure 39. Even with these obvious defects the individual layers were fused and delamination was no issue for the small parts printed.

Taking these results into consideration it was found to be incompatible for printing on the standard off-the-shelf hot end used. With slight compositional changes it may be possible to print with unmodified parts.

8. Conclusion and recommendations

Melt processing of the compositions was achieved. Even though initial compounding utilised solvent based methods it was shown that solvents could be entirely removed from the process. This is beneficial as it potentially reduces production costs by reducing chemical demands, as well as reducing the amount of volatile potentially hazardous compounds being released into the workplace and environment.

FK-800® was found to be a better oxidiser in this instance. Since its burn rates were more consistent especially when compared to that of Dyneon 31508®. However in both cases an additive is suggested for reducing the melt viscosity of the composition. LFC-1® did assist in improving the extrusion of filament for the oxidisers investigated in this study. A secondary benefit of adding the additive was that it increased burn rate and temperature. This is thought to be due to lowering the ignition temperature of the composition. The lower ignition temperature assists in speeding up the progression of the flame front from to the next layer of the composition by lowering the resistance to the reaction.

Aluminium was the choice fuel in this instance as simulations had indicated that it had better energetic performance than the alternative investigated. It was also deemed to be a safer fuel when considering the production products. For both fuels hydrofluoric and hydrochloric acid production can be suppressed by increasing the fuel load. Silicon however reacts with fluorine to form silicon tetrafluoride which may limit its possible uses as a fuel due to the dangers associated with it. Porous silicon powders may provide significant energetic bonuses if it can be produced in a cost effective manner.

It was shown that the compositions could be 3D printed though it was of a lower quality than observed with more traditional 3D printing materials. This opens up various possibilities for applications such as time delays and motors. Printing the fluoropolymers investigated did require several adjustments to be made to an off the shelf FDM type 3D printer. This was due to the greater resistance to flow that these polymers have when compared to the more commonplace 3D printing materials. Thermal conductivity was another issue that came to the front during printing. It was argued that this was due to the high aluminium content of the

compositions, which would cause significant heat transfer up the filament causing softening and swelling in the feeder tube. Improvements need to be made to the heat dissipation rate at the feed section of the hot end.

It is recommended that a lower fuel load be investigated in future. This could potentially improve the results by lowering the melt viscosity as well as lowering the thermal conductance of the system which may make it possible to produce prints of comparable quality to that of the more commonplace printing materials. Furthermore the effect of that printing density and geometry has on burn rates should be investigated.

9. References

Agrawal, J. P. 2010. *High Energy Materials Propellants, Explosives and Pyrotechnics,* Weinheim ,Wiley.

Akhavan, J. 2004. *The Chemistry of Explosives,* Cambridge, The Royal Society of Chemistry.

BariSin, D. & BatiniC-Haberle, I. 1994. "The influence of the various types of binder on the burning characteristics of the magnesium-, boron-, and aluminum-based igniters" *Propellants, Explosives, Pyrotechnics,* 19**,** 127-132.

Berger, B. 2005. "Parameters influencing the pyrotechnic reaction" *Propellants, Explosives, Pyrotechnics,* 30**,** 27-35.

Churaman, W., Currano, L. & Becker, C. 2010. "Initiation and reaction tuning of nanoporous energetic silicon" *Journal of Physics and Chemistry of Solids* 71**,** 69-74.

Clément, D., Diener, J., Gross, E., Künzner, N., Timoshenko, V. Y. & Kovalev, D. 2005. "Highly explosive nanosilicon-based composite materials" *Phsica Status Solidi,* 202**,** 1357-1364.

Conkling, J. A. 1985. *Chemistry of Pyrotechnics Basic Principles and Theory*, New York, Marcel Dekker

Cowgill, A. W. 2017. *The viability of poly(chlorotrifluoroethylene-co-vinylidene fluoride) as an oxidiser in exrudable pyrotechnic compositions.* Master of Engineering (Chemical)

Dombe, D., Mehilal, Bhongale, C., Singh, P. P. & Bhattacharya, B. 2015."Application of twin screw extrusion for continuous processing of energetic materials" *Central European journal of energetic Materials,* 12**,** 507-522.

du Plessis, M. 2008. "Nanoporous silicon explosive devices" *Materials Science and Engineering B,* 147**,** 226-229.

du Plessis, M. 2014."A decade of porous silicon as nano-explosive material" *Propellants, Explosives, Pyrotechnics,* 39**,** 348-364.

Fang, X. & Ahmad, S. R. 2016."Laser ignition of an optically sensitised secondary explosive by diode laser" *Central European Journal of Energetic Materials,* 13**,** 103-115.

Farrell, D., Limaye, S. Y. & Subramanian, S. 2006. *Porous silicon particles*, US patent application 11/381,777.

Fleck, T. J., Murray, A. K., Gunduz, I. E., Son, S. F., Chiu, G. T.-C. & Rhoads, J. F. 2017. "Additive manufacturing of multifunctional reactive materials" *Additive Manufacturing***,** 176-182.

Hough, M. 1995. *The Plastics Compendium*, Shawbury, Rapra Technology Limited.

Huong, C., Jian, G., DeLisio, J. B., Wang, H. & Zachariah, M. R. 2014."Electrospray deposition of energetic polymer nanocomposites with high mass particle loadings: a prelude to 3D printing of rocket motors" *Advanced Engineering Materials*, 17**,** 95-101.

Koch, E.-C. 2002. "Metal-Fluorocarbon-Pyrolants: III. Development and application of magnesium/Teflon/Viton (MTV)" *Propellants, Explosives, Pyrotechnics,* 27**,** 262-266.

Koch, E.-C. 2012. *Metal-Fluorocarbon Based Energetic Materials,* Weinheim, Wiley.

Koch, E.-C. & Clément, D. 2007. "Special materials in pyrotechnics: VI. silicon - an old fuel with new perspectives" *Propellants, Explosives, Pyrotechnics,* 32**,** 205-212.

Kolasinski, K. W. 2009. "Etching of silicon in fluoride solutions" *Surface science,* 603, 1904-1911.

Kubota, N. & Serizawa, C. 1987. "Combustion process of Mg/TF pyrotechnics" *Propellants, Explosives, Pyrotechnics,* 12**,** 145-148.

Loni, A., Barwick, D., Batchelor, L., Tunbridge, J., Han, Y., Li, Z. & Canham, L. 2011. "Extremely high surface area metallurgical-grade porous silicon powder prepared by metal-assisted etching" *Electrochemical and Solid-State Letters,* 14**,** K25-K27.

Moghaddam, A. Z. & Rees, G. J. 2003. "Thermoanalytical studies on pyrotechnic reactions" *Scientia Iranica,* 10**,** 267-272.

Osborne, D. T. & Pantoya, M. L. 2007. "Effect of Al particle size on the thermal degradation of Al/Teflon mixtures" *Combustion Science and Technology,* 179**,** 1467-1480.

Osswald, T. A. 2011. *Understanding Polymer Processing Processes and Governing Equations,* Munich, Hanser.

Pantoya, M. L. & Granier, J. J. 2005. "Combustion behavior of highly energetic thermites: nano versus micron composites" *Propellants, Explosives, Pyrotechnics,* 30, 53-62.

Plummer, A., Kuznetsov, V., Joyner, T., Shapter, J. & Voelcker, N. H. 2011. "The burning rate of energetic films of nanostructured porous silicon" *Small,* 7, 3392-3398.

Poling, B. E., Thompson, G. H., Friend, D. G., Rowley, R. L. & Wilding, W. V. 2008. *Perry's Chemical Engineers' Handbook, 8th edition,* New York, McGraw-Hill.

Priedeman, W. R. J. 2011. *Build materials containing nanofibres for use with extrusion-based layerd deposition systems*. United States patent application 12/001,403.

Prokes, S. M. 1996. "Surface and optical properties of porous silicon" *Journal of Materials Research* 11, 305-320.

Sailor, M. J. 2012. *Porous Silicon in Practice: Preperation, Charecterization and Applications,* 1st edition, Weinheim Germany, Wiley-VCH.

Searson, P. C., Macaulay, J. M. & Prokes, S. M. 1992. "The formation, morphology, and optical properties of porous silicon structures" *The Electrochemical Society* 139, 3373-3378.

Subramanian, S., Tiegs, T., Limaye, S., Kapoor, D. & Redner, P. 2008. *Nanopourous silicon based energetic materials*. Vesta Sciences, NJ 08852.

Teipel, U. 2005. *Energetic Materials Particle Processing and Characterization,* Weinheim, Wiley.

Teng, H. 2012. "Overview of the development of the fluoropolymer industry" A*pplied Sciences,* 2, 496-512.

Terry, B. C., Lin, Y.-C., Manukyan, K. V., Mukasyan, A. S., Son, S. F. & Groven, L. j. 2014. "The effect of silicon powder characteristics on the combustion of silicon/Teflon/Viton nanoenergetics" *Propellants, Explosives, Pyrotechnics,* 39, 337-347.

Trucks, G. W., Raghavachari, K., Higashi, G. S. & Chabal, Y. J. 1990. "Mechanism of HF etching of silicon surfaces: a theoretical understanding of hydrogen passivation" *Physical Review Letters,* 65**,** 504-507.

Weismiller, M. R., Malchi, J. Y., Lee, J. G., Yetter, R. A. & Foley, T. J. 2011. "Effect of fuel and oxidizer particle dimensions on the propagation of aluminum containing thermites" *Proceeding of the Combustion Institute,* 33, 1989-1996.

Yarrington, C. D. & Son, S. F. 2010. "Combustion of silicon/Teflon/Viton and aluminum/ Teflon/Viton energetic composites" *Journal of Propulsion and Power,* 26, 734-743.

Yen, N. H. & Wang, L. Y. 2012. "Reactive metals in pyrotechnics" *Propellants, Explosives, Pyrotechnics,* 37**,** 143-155.

Yetter, R. A., Risha, G. A. & Son, S. F. 2009. "Metal particle combustion and nanotechnology" *Proceedings of the Combustion Institute,* 32**,** 1819-1838.

Zhang, X., Collins, S. & Smith, R. 1989. "Porous silicon formation and electropolishing of silicon by anodic polarization in HF solution" *Journal of the Electrochemical Society,* 136**,** 1561-1565.